Turkish Journal of Chemistry

Volume 45 | Number 1 Article 15

1-1-2021

Novel nonperipheral octa-3-hydroxypropylthio substituted metallo-phthalocyanines: synthesis, characterization, and investigation of their electrochemical, photochemical and computational properties

NİLGÜN KABAY

YASEMİN BAYĞU

METİN AK

İZZET KARA

ESRA NUR KAYA

See next page for additional authors

Novel nonperipheral octa-3-hydroxypropylthio substituted metallo-phthalocyanines: synthesis, characterization, and investigation of their electrochemical, photochemical and computational properties

Authors
NİLGÜN KABAY, YASEMİN BAYĞU, METİN AK, İZZET KARA, ESRA NUR KAYA, MAHMUT DURMUŞ, and YAŞAR GÖK

TÜBİTAK

Turkish Journal of Chemistry

http://journals.tubitak.gov.tr/chem/

Research Article

Turk J Chem
(2021) 45: 143-156
© TÜBİTAK
doi:10.3906/kim-2008-48

Novel nonperipheral octa-3-hydroxypropylthio substituted metallo-phthalocyanines: synthesis, characterization, and investigation of their electrochemical, photochemical and computational properties

Nilgün KABAY[1,*], Yasemin BAYGU[2], Metin AK[3], İzzet KARA[4], EsraNur KAYA[5], Mahmut DURMUŞ[5], Yaşar GÖK[6]

[1]Department of Biomedical Engineering, Pamukkale University, Denizli, Turkey
[2]Tavas Vocational School of Higher Education, Pamukkale University, Denizli, Turkey
[3]Department of Chemistry, Pamukkale University, Denizli, Turkey
[4]Department of Physical Education, Pamukkale University, Denizli, Turkey
[5]Department of Chemistry, Gebze Technical University, Kocaeli, Turkey
[6]Department of Chemical Engineering, Uşak University, Uşak, Turkey

Received: 26.08.2020 • **Accepted/Published Online:** 04.11.2020 • **Final Version:** 17.02.2021

Abstract: The current study describes the synthesis, electrochemical, computational, and photochemical properties of octa (3-hydroxypropylthio) substituted cobalt (II) (**4**), copper (II) (**5**), nickel (II) (**6**) and zinc(II) (**7**) phthalocyanine derivatives. These novel compounds were characterized by elemental analysis, ^{1}H, ^{13}C NMR, FT-IR, UV-Vis, and MS. The redox behaviors of these metallo-phthalocyanines were investigated by the cyclic voltammetric method. The optimized molecular structure and gauge-including atomic orbital (GIAO) ^{1}H and ^{13}C NMR chemical shift values of these phthalocyanines in the ground state had been calculated by using B3LYP/6–31G(d,p) basis set. The outcomes of the optimized molecular structure were given and compared with the experimental NMR values. The photochemical properties including photodegradation and singlet oxygen generation of zinc(II) phthalocyanine were studied in DMSO solution for the determination of its photosensitizer behaviors.

Key words: Metallo-phthalocyanines, cyclic voltammetry, computational chemistry, photodynamic therapy, photochemical properties

1. Introduction

Phthalocyanines (Pcs) and their metal complexes have been studied for a long time, and they are still the matters of intense investigation. They show various exceptional properties and they havepotential applications in different scientific and innovative areas like nonlinear optics [1], electrochromic imaging systems [2], chemical detectors [3–5], solar cells [6], photovoltaic optics, molecular electronics [7], liquid crystals [8], semiconductors [9], laser dyes [10], optical storage devices [11], catalyst [12] and photodynamic therapy (PDT) [13]. The developing utilization of phthalocyanines as cutting edge materials in the recent decade and they have empowered the blend of new materials which vary as far as the central metal ion and peripheral substituents [14].

Electrochemical properties of phthalocyanines in the electrolytic solution, are dependent ontheir energy values of the HOMOs and LUMOs of the frontier orbitals [15]. Electrochemical properties of the proposed compounds may have the possible potential usage in electrocatalysis, electrosensing, and electrochromic devices. Electron donating alkylthio substituted phthalocyanines are also inherently electron-rich p-type semiconductors [16,17].

The numerous applications of zinc(II) phthalocyanines in the field of medicine, molecular electronics, magnetic devices, chemical sensors depend on their photophysical and photochemical properties. The photochemical properties of these compounds, especially, singlet oxygen quantum yield and photostability were also investigated for photodynamic therapy applications [18]. Therefore, they are widely used in cancer treatment as novel generation photosensitizers. Photosensitizers are desirable to have a long wavelength. In this manner, they have an effective curing performance over deep skin cancer types. However, due to having low energy, photosensitizers decrease the possible harmful effect of light irradiation. [19,20]. Phthalocyanines were known as second-generation photosensitizers in PDT of cancer. They have long-wavelength absorption and highly effective singlet oxygen generation abilities. For this reason, they are suitable for use in cancer treatment [21].

* Correspondence: nerkalkabay@pau.edu.tr

In this study, the novel metallo-phthalocyanines wherein the 3-hydroxypropylthio groups connected to nonperipheral positions of the Pc macrocycle were synthesized. Electron donating sulfur groups are known to shift the Q-band to the long wavelength in nonperipheral positions that is desirable for potential PDT applications. The newly synthesized compounds have been characterized by ^{1}H, ^{13}C NMR, UV-Vis, FT-IR, micrOTOF mass, electrochemical and computational studies as well as elemental analysis. The photochemical properties such as singlet oxygen generation and photodegradation of zinc(II) phthalocyanine was also investigated to determine possible usage of this compound as a photosensitizer for cancer treatment by photodynamic therapy technique. The theoretical ^{1}H and ^{13}C NMR data of the optimized geometry were also compared with the experimental chemical shift values.

2. Experimental

All information about the used materials, equipment, synthesis, electrochemical measurements singlet oxygen and photodegradation quantum yields as photophysical properties and theoretical calculations were showed in the "Supplementary materials".

3. Results and discussion

3.1. Synthesis and characterization

3,6-bis(3-hydroxypropylthio)phthalonitrile (**3**) was synthesized via a condensation reaction of 3,6-dibromophthalonitrile [22] with 3-mercapto propanol under very convenient conditions with a better yield than the first synthesis result (38%) (Scheme 1) [23]. This compound was prepared previously by the S_NAr reaction of 3,6-(4'-methylphenyl-sulfanyloxy) phthalonitrile with 3-mercapto-propanole. In the ^{1}H NMR spectrum of this compound, resonances at δ = 3.49, 1.73, 3.17, and 4.67 ppm should be related to OCH_2, CH_2, SCH_2, and –OH protons, respectively. The aromatic protons appeared as a dublet at δ = 7.81–7.78 ppm as expected (Figure S1). ^{13}C NMR spectrum of **3** showed the presence of characteristic carbon

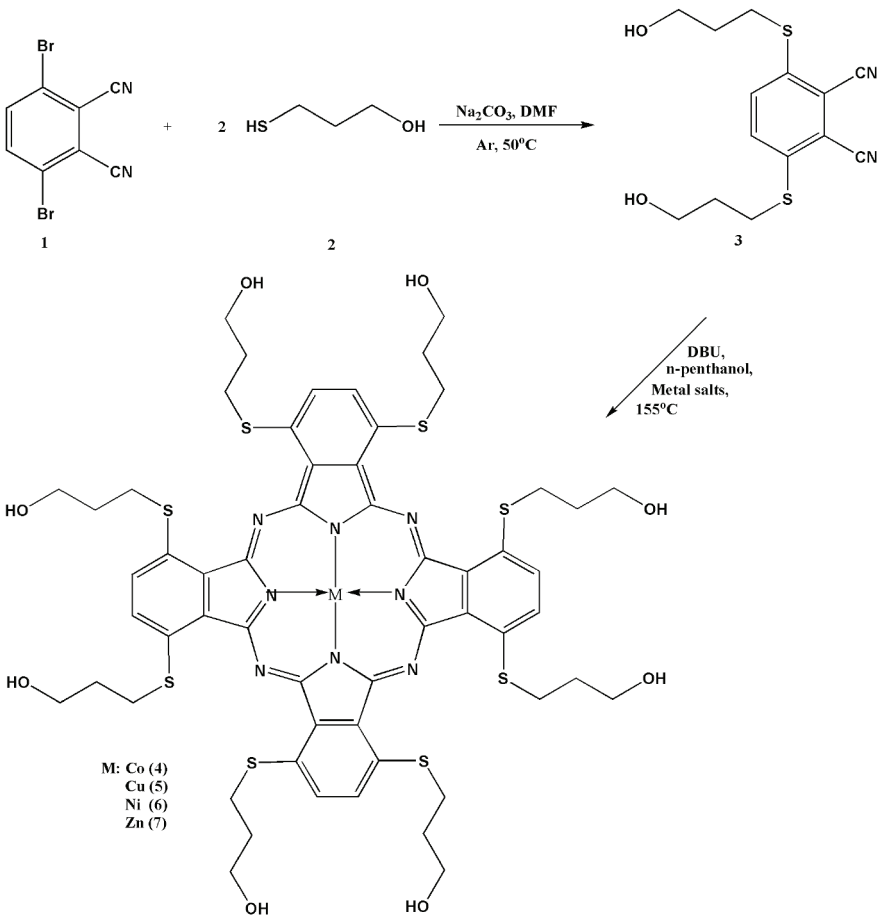

Scheme 1. The synthesis route of the phthalonitrile and metallophthalocyanines.

resonances of C≡N groups at δ = 116.95 ppm, that can be attributed to the formation of 3,6-disubstituted phthalonitrile. The other chemical shifts at δ = 132.9, 141.2, 145.3, 59.6, 31.9, and 29.7 ppm could be related CN-ArC, ArC, S-ArC, OCH_2, SCH_2, and CH_2 moieties, respectively (Figure S2). These NMR signals (Table 1) are in accordance with the published results [23]. In the FT-IR spectrum of this molecule showed the characteristic vibrations for the C≡N groups at 2220 cm^{-1} (Figure S3).

Metallo-phthalocyanines (**MPc**) (**4–7**) were synthesized by the reaction of **3** with anhydrous metal salts ($CoCl_2$, $NiCl_2$, $CuCl_2$, and $Zn(OAc)_2$) in *n*-pentanol in the presence of catalytic amounts of DBU under an argon atmosphere (Scheme 1). The shared features of all new products were performed by spectroscopic methods and elemental analysis such as UV-Vis, FT-IR, ^{1}H NMR (for compounds **3**, **6,** and **7**), ^{13}C NMR (for compounds **3** and **7**) and MS (micrOTOF).

In the ^{1}H NMR spectra of nickel(II) (**6**) and zinc(II) (**7**) phthalocyanines in DMSO-d_6, the characteristic resonances of aromatic protons were observed at δ = 7.74–7.58 or 7.98 ppm, respectively. The other signals of compound **6** and **7** due to hydroxypropyl groups as multiplets at δ = 1.95 (**6**) or singlet at 2.11 ppm (**7**) for -CH_2- protons, broad chemical shift at δ = 3.66 (**6**) and dublet at 3.77 ppm (**7**) for OCH_2 protons, broad singlet at δ = 3.33 (**6**) ppm as superimposed H_2O proton, and singlet δ = 3.45 (**7**) ppm for SCH_2 protons and broad peaks at δ = 4.70 (**6**), 4.75 (**7**) ppm concerning OH (Figures S4 and S5). ^{13}C NMR spectra concerning C≡N signals at δ = 116.9 ppm belonging to precursor compound (**3**) disappeared in the case of **NiPc** and **ZnPc** formations. In addition to that, the appearance of novel signals at δ = 145.5 ppm and δ = 152.7 related to the inner core of phthalocyanines also indicated the formulation of metallo-phthalocyanine structures (Figures S6 and S7). The other ^{13}C NMR data of these molecules were almost identical to those of the precursor molecule (**3**) as anticipated. In the MS spectra of **NiPc** and **ZnPc** measured by the micrOTOF technique proved proposed structure due to the molecular ion peaks which observed at *m/z* = 1291.9 $[M]^+$ and 1298.9 $[M]^+$, respectively (Figures S8 and S9). In the FT-IR spectra of the compounds (**4–7**) (Figures S10–S13), the stretching vibrations concerning C≡N groups at 2221 cm^{-1} belong to phthalonitrile (**3**) disappear after the cyclotetramerization reaction. The deformation of these vibrations confirmed the formation of phthalocyanines. The rest of the FT-IR spectra showed very close similarity to the starting compound. The mass spectra of compounds **4** and **5** recorded by micrOTOF technique also confirmed the molecular ion peaks at *m/z* = 1291.0 $[M+H]^+$ and 1297.2 $[M]^+$, respectively (Figures S14 and S15).

Theoretical ^{1}H and ^{13}C NMR chemical shifts of the compound **3** and **ZnPc** were calculated from B3LYP/6–31G (d,p) (see in the optimized molecular structure of the **ZnPc** in the ground state, Figure 1). The calculated NMR resonances concerning phthalonitrile compound **3** and **ZnPc** were given in Tables 1 and 2, respectively. The optimized geometric parameters of the **ZnPc** compound (bond lengths, bond angles, and dihedral angles) by B3LYP methods with 6–31G(d,p) as the basis set were presented in Tables S1 and S2. The correlations (Figure 2) between the experimental and calculation of

Table 1. ^{1}H and ^{13}C chemical shifts of compound **3** (experimental and theoretical values).

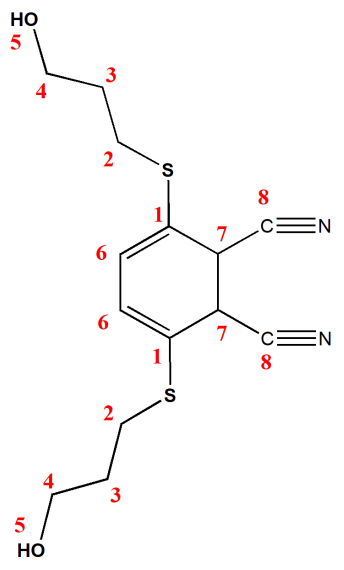

Atoms	Exp.	Gas phase	DMSO
C_1	145.27	141.99	143.74
C_2	31.87	32.06	32.31
C_3	29.74	32.13	32.39
C_4	59.55	62.29	61.59
C_6	132.99	119.57	123.10
C_7	141.15	113.72	111.04
C_8	116.05	105.13	108.02
H_2	3.17	2.08	3.08
H_3	1.73	2.74	1.98
H_4	3.49	4.01	4.02
H_5	4.67	0.19	0.80
H_6	7.81	7.11	7.63

Table 2. ^{1}H and ^{13}C chemical shift of **ZnPc** (experimental and theoretical values).

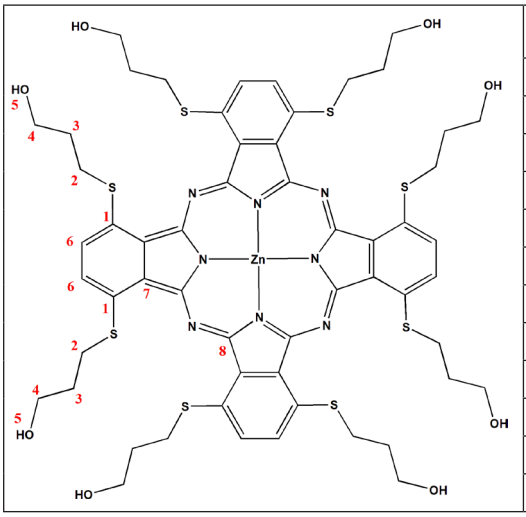

Atoms	Exp.	Gas phase	DMSO
C_1	133.66	135.07	134.94
C_2	32.26	32.36	32.78
C_3	28.23	33.48	34.10
C_4	60.41	63.14	62.96
C_6	125.57	117.07	119.32
C_7	132.69	132.46	130.59
C_8	152.68	148.46	149.21
H_2	3.45	3.07	3.19
H_3	2.11	2.46	2.19
H_4	3.77	4.07	4.08
H_5	4.75	0.19	0.75
H_6	7.98	7.79	7.99

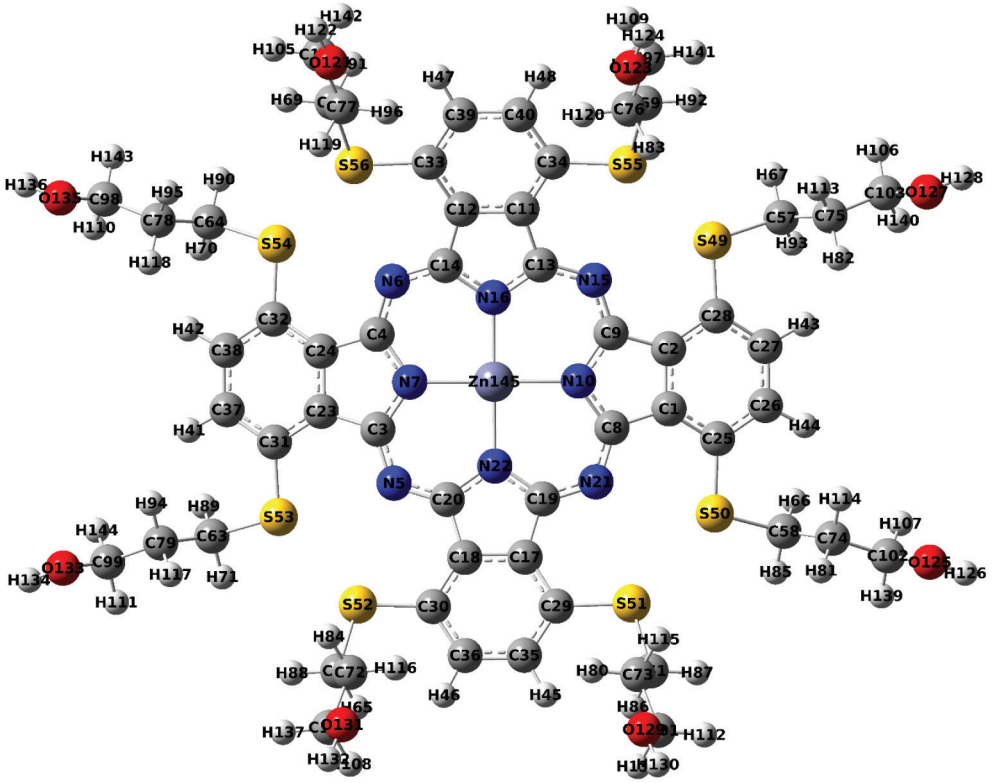

Figure 1. Optimized geometry of the **ZnPc** in the ground state.

the chemical shift values of the compounds are described by the equations of d_{cal} (ppm) = 0,953 d_{exp} + 0,6972 (R^2 = 0,983) for compound **3** (Table 1) and d_{cal}(ppm) = 0,9738 d_{exp} + 0,6852 (R^2 = 0,9915) for **ZnPc** (Table 2), respectively.

3.2. Ground state electronic absorption spectra

Phthalocyanine compounds show two strong absorption bands in their electronic absorption spectroscopy that correlate to $\pi \rightarrow \pi^*$ transitions. One of them is the so-called Q-band and seen at around 600–800 nm, and the other is called as B band and

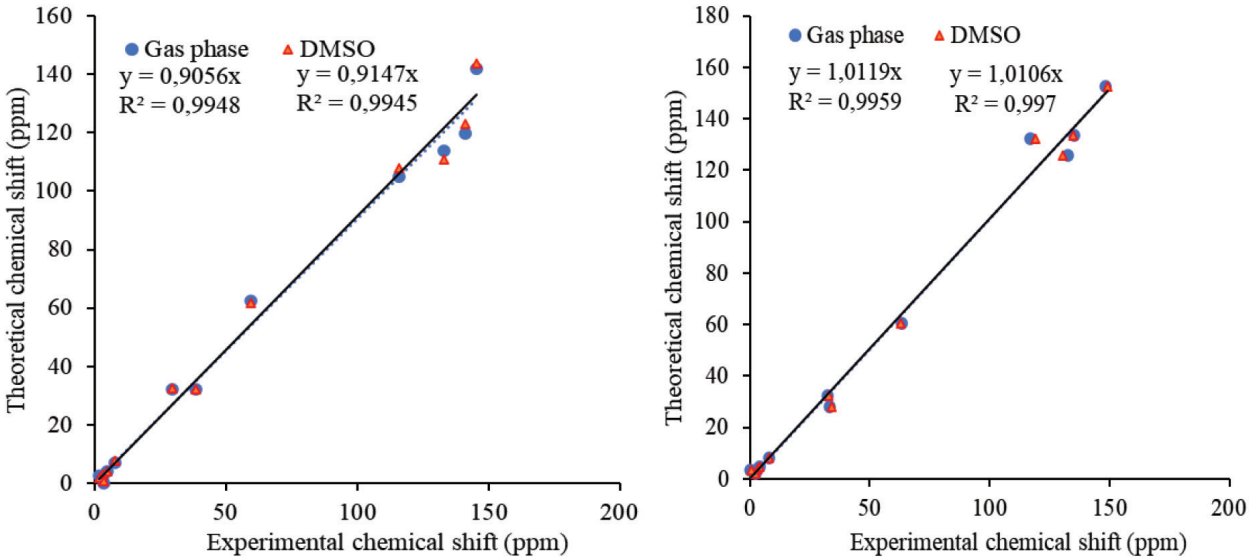

Figure 2. The correlation graphs between the experimental and theoretical ^{1}H and ^{13}C chemical shift values of the molecules in DMSO.

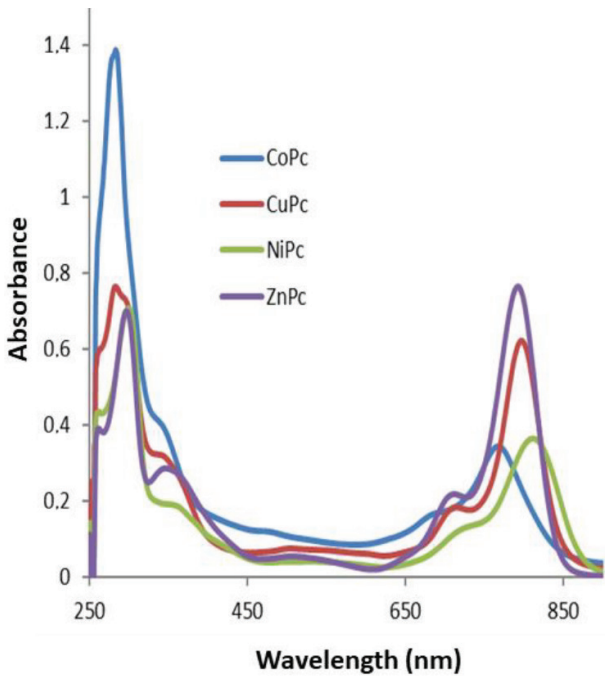

Figure 3. The UV-Vis spectra of **MPc** (1×10^{-5} M in DMSO).

arise approximately 300–450 nm [24]. The ground-state electronic absorption spectra of Ni(II), Co(II), Cu(II) and Zn(II) phthalocyanines were measured in DMSO (Figure 3). The most of phthalocyanines show characteristic absorption band in the visible region approximately at around 600–750 nm named the Q-band and in the UV region at around 300–400 nm named B or Soret band [25]. The Q-band absorption in DMSO of the four metallated phthalocyanine can be aligned in the sequence Ni(II) > Cu(II) > Zn(II) > Co(II). The Q-bands were seen at 811, 797, 792, and 767 nm for compounds **6**, **5**, **7**, and **4**, respectively. These single absorptions in lower energy regions should be related $\pi \rightarrow \pi^*$ transitions of the phthalocyanine cores. The Q-bands of compounds are significantly red-shifted among the metallo-phthalocyanines. It is well known that the electron-releasing groups such as alkylthio are bound to eight α-benzo positions of the phthalocyanine skeleton,

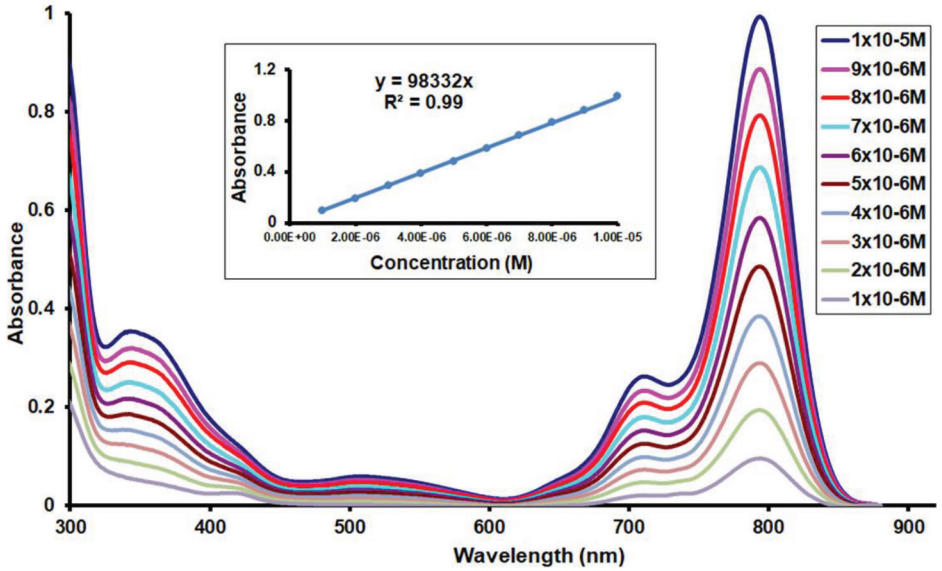

Figure 4. Electronic absorption spectral changes for complex **7** in DMSO at different concentrations (Inset: Plot of absorbance versus concentration).

the Q-band absorptions shift to longer wavelength. The transition metal ions have been settled in the phthalocyanine core may be expected they greatly affect absorption properties. Ni(II), Cu(II) and Co(II) have a similar electronegativity [26], so that the effect of electronegativity on the red-shifted is inferred to be similar [27]. The absorption maxima of **4** and **7** shifts to the shorter wavelength in the order of Co(II) and Zn(II) as central metals in the phthalocyanine core [28]. Ni(II) phthalocyanines have maximum red as an unusual shift among the metallatedphthalocyanines can be attributed the perfect planarity of the d^8 electronic configuration of this metal [14].

Aggregation is usually portrayed as a coplanar association of rings proceeding from monomer to dimer and higher order complexes. There are lots of parameters for aggregation in phthalocyanines; concentration, the nature of the solvent, nature of the substituents, complexed metal ions, and temperature [29]. The Q-band absorption maximum was independent of concentration and followed the Beer–Lambert law with a constant extinction coefficient in the studied concentration range [Figure 4 as an example for **ZnPc**(**7**)] for all studied metallo-phthalocyanines and these phthalocyanines did not exhibit any aggregation in the studied concentration range.

3.3 Electrochemical studies

Voltammetric analyses of metallo-phthalocyanines have been performed with cyclic voltammetry (CV) as mentioned above. Figure 5 demonstrates the CV responses of the synthesized metallo-phthalocyanines recorded in the cathodic and anodic potential side in DCM:DMF (0.8:0.2)/TBP_6 electrolyte system on an ITO working electrode.

CoPc gives nonquasi-reversible metal-based reduction at 0.25 V (R1). Also, it is thought that nonquasi-reversible Pc based oxidation and reduction reactions were observed at 0.1 V(O1) and –0.25 V(R2). Most of the studies in the literature on reduction properties of the MPc complexes including that such complexes have two reduction processes as one metal- and one ring-based [30,31].

Cyclic voltammetry graph of **NiPc** showed two oxidation peaks at 1.14 and 0.62 V and consecutive reduction peaks at 1.00 V and 0.38 V. When the electrochemical behavior of **CuPc** is examined, oxidation and reduction peak values have found to be lower than those of **NiPc**. In terms of **CuPc**, these values are 1.0 V and 0.56 V for oxidation and 0.18 V and 0.88 V for reduction. **ZnPc** had the lowest oxidation and reduction peak potential values among those of the other studied phthalocyanine derivatives. Compared to **NiPc** which has the oxidation peak values at 1.14 V and 0.62 V, **ZnPc** had lower redox peak values at 0.98 V and 0.49V. This result may be due to the smaller atomic radius of Zn metal comparing to the other metals' atomic radii.

The speed of the applied potential can be changed by changing the scan rate in cyclic voltammetry experiments. Higher peak current values were obtained at high scan rates due to a reduction in the size of the diffusion layer [32]. Figure 6 shows a series of cyclic voltammograms recorded at different scan rates for an electrolyte solution containing metallo-phthalocyanine. The linearity of the peak current values with the square root of the scan rates proved that the electrochemical reaction on the electrode surfaces was diffusion controlled as expected [32].

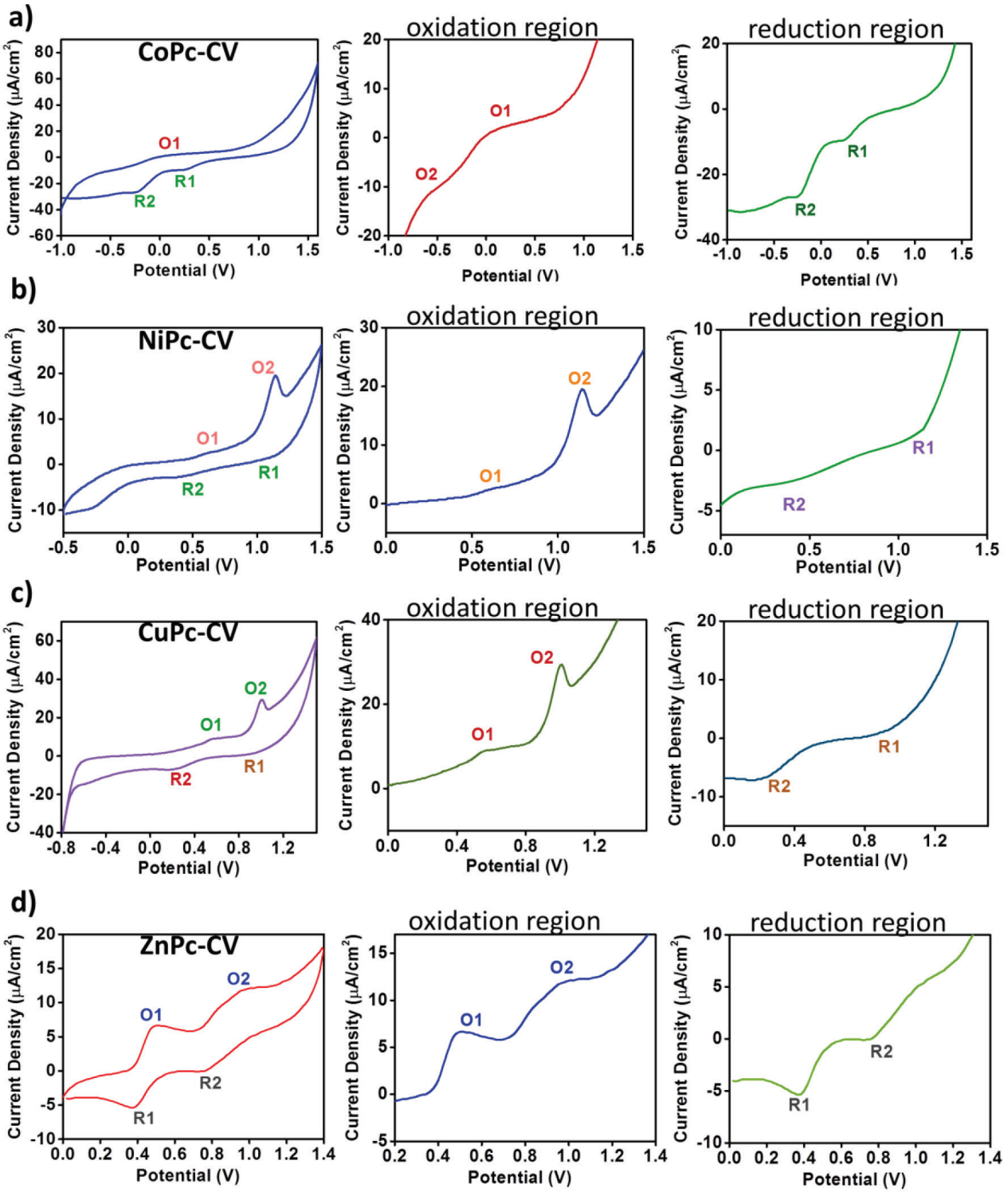

Figure 5. CV responses of synthesized metallo-phthalocyanines a) CoPc, b) NiPc, c) CuPc, d) ZnPc recorded in the cathodic and anodic potential side in DCM:DMF (0.8:0.2)/ TBP6 electrolyte system on an ITO working electrode.

3.4. HOMO-LUMO studies

The electrostatic potential map of a molecule supply knowledge about the electron acceptor and electron donor regions. This knowledge may help us to see the relationships between the atoms regarding intramolecular and intermolecular

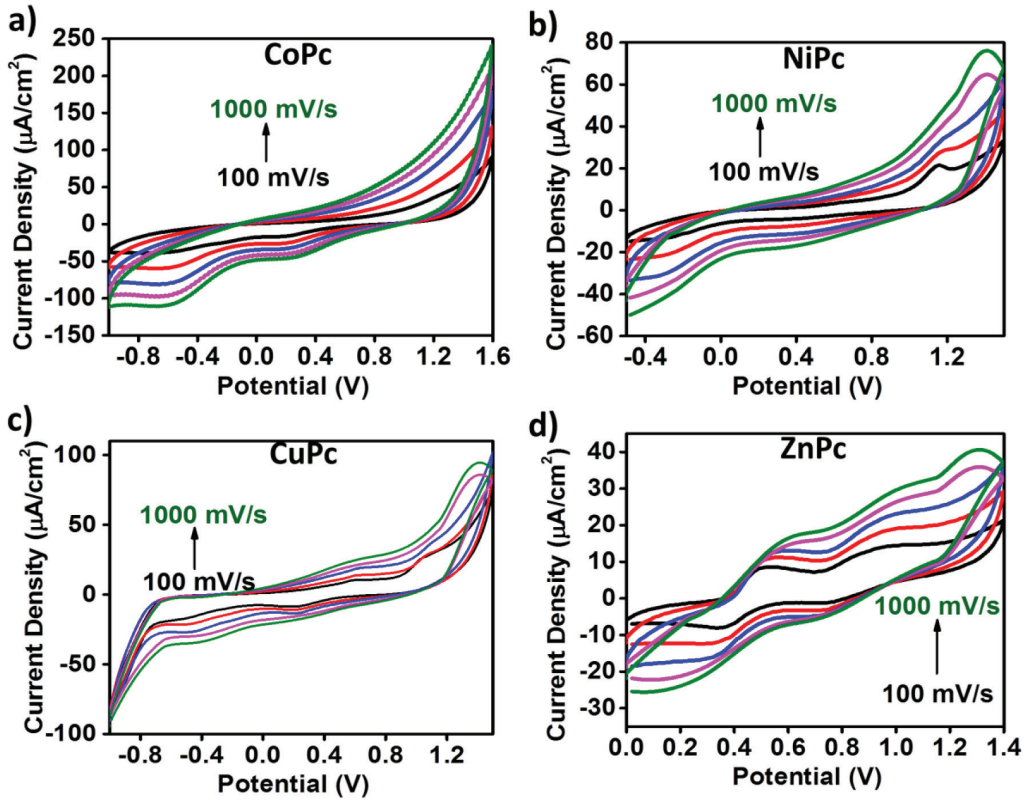

Figure 6. CV responses of synthesized metallo-phthalocyanines at different scan rates a) CoPc, b) NiPc, c) CuPc, d) ZnPc recorded in DCM:DMF (0.8:0.2)/TBP6 electrolyte system.

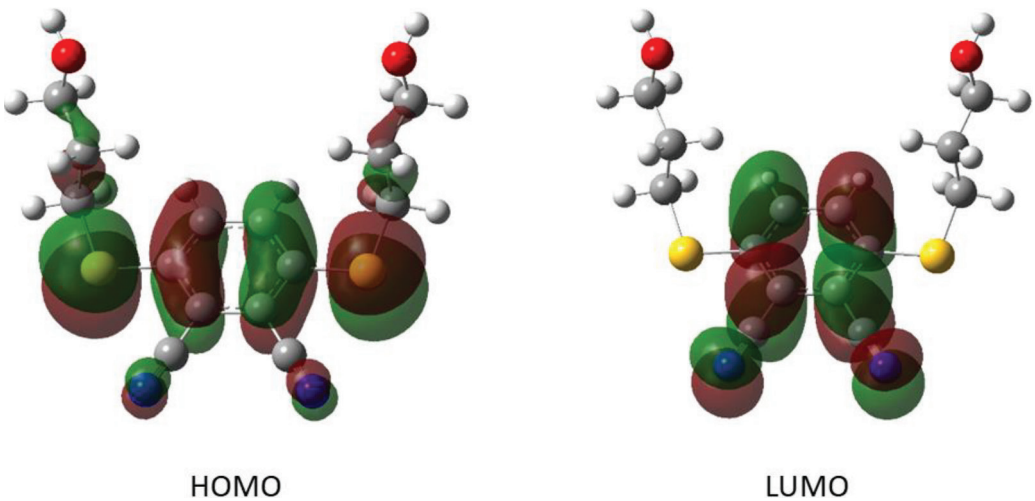

Figure 7. The HOMO and LUMO energies of the compound **3** with B3LYP/6–31G(d,p) basis set in gas phase.

hydrogen bonds. The distinctive values of the electrostatic potential at the area of the map are referred to by varied colours: blue refers to the most positive electrostatic potential, red refers to the most electronegative electrostatic potential site and green refers to the zero potential sites.

The electronic properties of a molecule can be calculated depending on HOMO and LUMO energies. In the calculations, the electron affinity (A=–LUMO) and the ionization potential (I=–HOMO) are the basic parameters. The other parameters such as absolute electronegativity (c=(I+A)/2), softness (S =(I-A)/2), and absolute hardness (h=(I-A)/2) can be calculated accordingly.

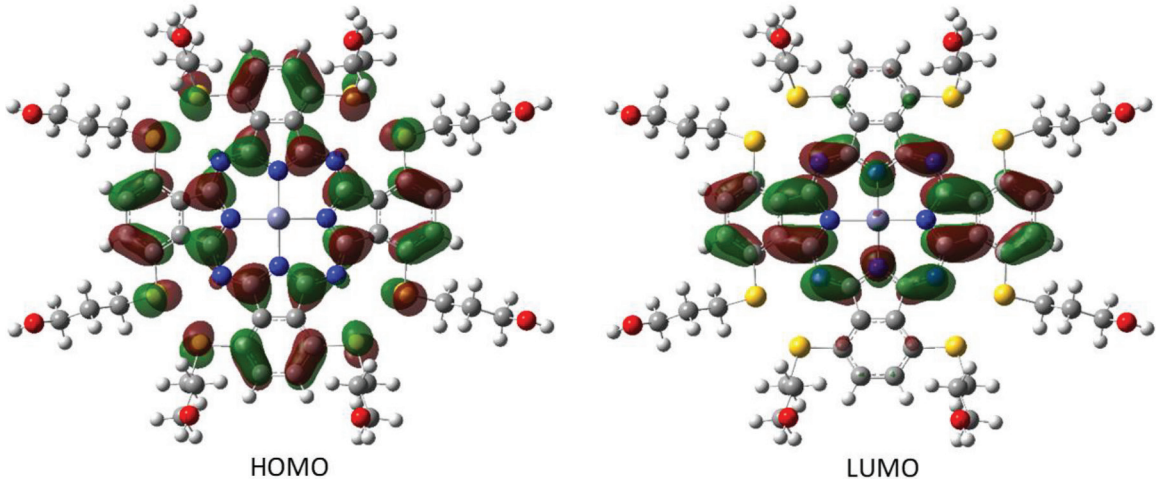

Figure 8. The HOMO-LUMO energies of the **ZnPc**.

Table 3. Electronic properties for the phthalonitrile **(3)** and **ZnPc** compounds.

	Phthalonitrile (**3**)			**ZnPc**		
Electronic parameters	6–31g(d)	6–31g(d,p)	6–31g+(d,p)	6–31g(d)	6–31g(d,p)	6–31g+(d,p)
eV	4.3009	4.2996	4.1644	1.6878	1.6857	1.6504
l(Å)	288.28	288.36	297.72	734.6	735.51	751.25
Oscillator strengths	0.1665	0.1458	0.2951	0.4347	0.4356	0.4374
HOMO (au)	–0.22186	–0.22195	–0.23012	–0.15748	–0.15774	–0.16678
LUMO (au)	–0.07989	–0.08017	–0.09137	–0.08906	–0.08939	–0.09940
ΔE=LUMO-HOMO	3.86	3.86	3.78	1.86	1.86	1.83
TD/LUMO-HOMO	4.30	4.30	4.16	1.69	1.69	1.65
I (eV)	6.04	6.04	6.26	4.29	4.29	4.54
A (eV)	2.17	2.18	2.49	2.42	2.43	2.70
χ (eV)	4.11	4.11	4.37	3.35	3.36	3.62
Hardness(η)	1.93	1.93	1.89	0.93	0.93	0.92
Softness(s)	0.52	0.52	0.53	1.07	1.08	1.09
μ = -(I + A)/2 = - χ	–1.93	–1.93	–1.89	–0.93	–0.93	–0.92
ω = μ2 / (2η)	0.966	0.965	0.944	0.465	0.465	0.458
Dipole moment (debye)	12.084518	12.036222	12.379576	6.017804	5.869903	7.233204
Polarizability (α) (a.u)	211.008667	212.453118	237.359667	724.789333	729.525000	792.483000
Hyperpolarizability (β) (a.u)	214.054379	215.011406	574.413256	387.135619	394.940022	1518.758510

The dispersions of the HOMO and LUMO orbitals calculated for the B3LYP/6–31G(d, p) level for the compounds **3** and **ZnPc** were shown in Figures 7 and 8, respectively. In our calculations, **ZnPc** had a total of 1588 orbitals out of which 339 were filled and the rest were 1249 empty orbitals. The orbital numbered as 339 accounted for HOMO and 340 accounted for LUMO orbitals. The corresponding energy values were calculated as –4.29 eV for the HOMO and –2.42 eV for the LUMO energies with B3LYP/6–31G(d, p) level. The parameters for the 3,6-bis-(3-hydroxypropylthio)phthalonitrile were calculated at the same levels and the results were presented in Table 3.

As shown in Figure 9, the red region was localized on the nitrogen atoms and vicinity of the sulphur atoms in both the phthalonitrile and the **ZnPc**, whereas the blue region was delocalized on the OH groups. Hence, it was found that the

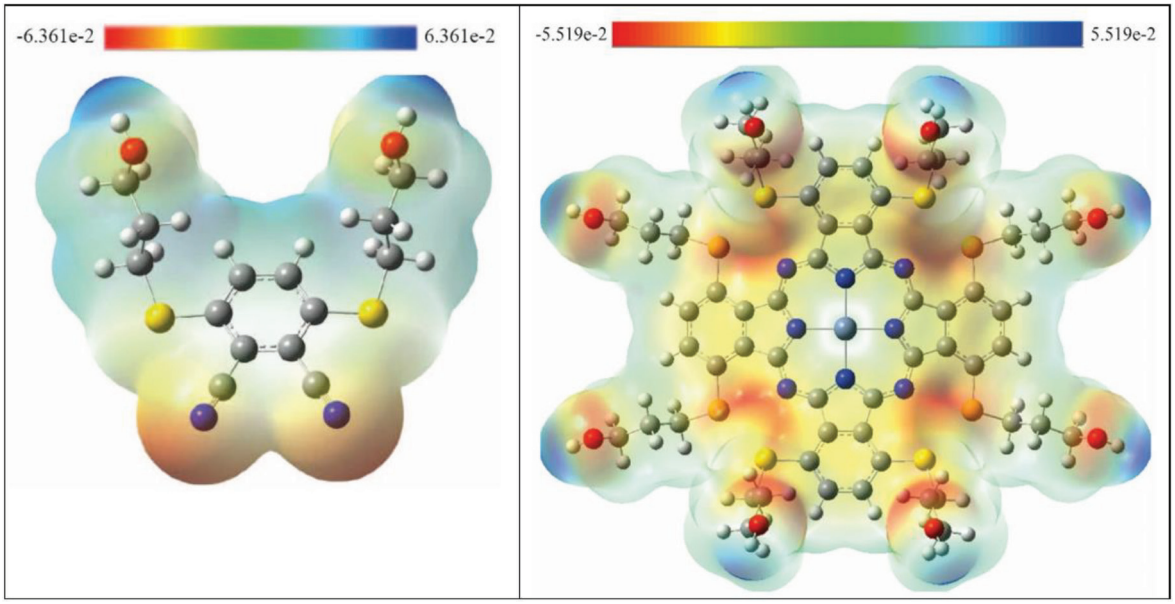

Figure 9. The MAP surface obtained at B3LYP/6–31G(d,p) level for phthalonitrile and **ZnPc** compounds.

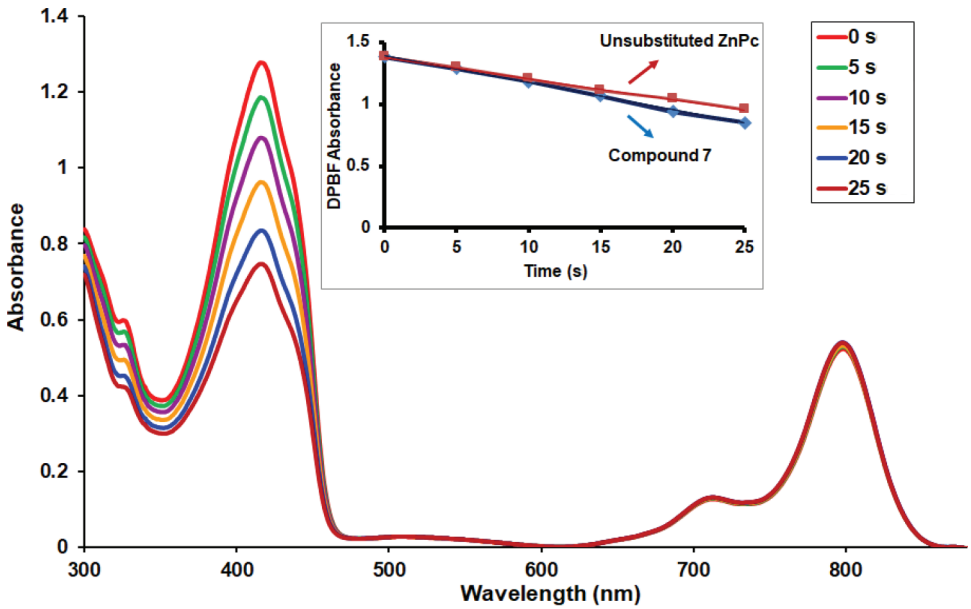

Figure 10. Electronic absorption spectral changes during singlet oxygen determination. This determination was for compound **7** in DMSO at a concentration of 1.0×10^{-5} M using DPBF at a concentration of 1.0×10^{-4} M (Inset: Plot of DPBF absorbance versus time).

ZnPc was useful to both bond metallically, and it has intermolecularly interacted. This result also supports the evidence of the charge analyses part.

NBO analysis is a tool for the determination of intramolecular interactions. The NBO analysis is used to specify the interactions between filled and empty orbitals of a molecule with the help of DFT method [33–35]. The NBO analysis, especially charge transfer, indicates the role of intermolecular orbital interaction in the compound. In tandem with this, the stabilization energy $E^{(2)}$ linked with electron delocalization between donor and acceptor is predicted for each donor NBO (i) and acceptor NBO (j) as follows:

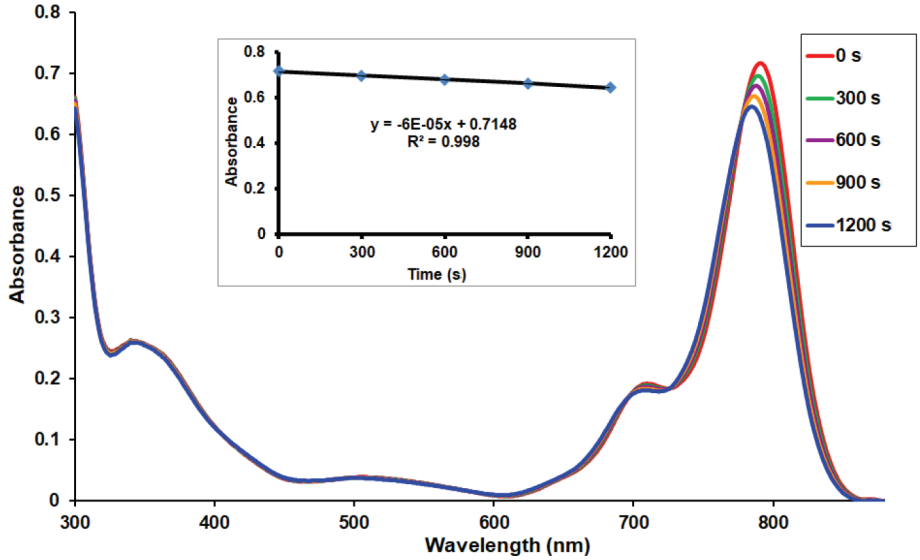

Figure 11. The electronic absorption spectral changes of zinc(II) phthalocyanine (**7**) in DMSO under light irradiation revealing the vanishing of the Q-band at 5 min intervals (Inset: Plot of absorbance vs. time).

$$E^{(2)}=\Delta E_{ij}=q_i \frac{F^2_{(i,j)}}{E_j-E_i}$$

where q_i is the orbital occupancy of the i^{th} donor, E_j and E_i are the diagonal elements (orbital energies) and $F_{(i,j)}$ is the off-diagonal NBO Fock matrix element. The hyper conjugative σ→σ* interactions play an extremely significant role in the molecule represent the weak departures from a strictly localized natural Lewis structure that constitutes the primary "noncovalent" effects [36]. The results of the NBO analysis of the **ZnPc** collected with B3LYP/6–31G(d,p) basis set presented in Table S3.

The interactions between C25-C26 (π*) and π*(C1-C2), C27-C28 (π*) and π*(C1-C2), the stabilization of 275.24 kcal/mol, which denotes larger delocalization. According to Table S3, C25-C26 is rich in electrons since close to the electron release group. That is why it is a donor. In contrast, C1-C2 is acceptor because the electron is poor. The interaction between the C8-N10 (σ*) π*(C19-N21), C3-N5 (π*) π*(C23-C31), C4-N7 (π*) π*(N6-C14), C13-N16 (π*) π*(C9-N15), C19-N21 (π*) π*(C17-C29), C20-N22(π*) π*(C3-N5) also represent the larger delocalization. The $E^{(2)}$ value is essential chemically and may be exploited as a measure of the intramolecular delocalization.

The calculated visible absorption maxima at TD–B3LYP/6–31G(d,p) of λ which are a function of the electron availability were displayed in Table 3. The most likely transition for the molecule is the HOMO-LUMO transition at 339→340 because the maximum f = 0.4356 (oscillator strength) value is in the excited state-1 at 735.51 nm. HOMO-LUMO+1 transition was calculated at 339→341 molecular orbital, excited state-2: 735.21 nm. Typically, the energy bandgap in inorganic materials is ~ 1.5 eV, in organic materials is in the range of 1.5–3.5 eV. In accordance with this, the compound is capable of being a potential molecule for inorganic semiconductor materials [37]. Additionally, according to ligand, this value reveals that the compound becomes more conductive electrically.

3.5. Singlet oxygen generation properties

PDT is a treatment for cancer where light, molecular oxygen, and photosensitizer are used in combination to produce cytotoxic forms of oxygen such as singlet oxygen. The generation of singlet oxygen is the key to show PDT potential of the compounds [38]. The singlet oxygen production of studied zinc(II) phthalocyanine (**7**) was determined with the chemical method in DMSO. 1,3-diphenylisobenzofuran (DPBF) was used as a singlet oxygen scavenger which causes the formation of endoperoxide species. A time-dependent decrease of DPBF absorbance at 417 nm was observed for phthalocyanine photosensitizer **7**. There was no change in the Q-band intensity during the Φ_Δ determinations and it supports that studied phthalocyanine did not show any degradation by used light irradiation (Figure 10). The singlet oxygen production of studied zinc(II) phthalocyanine (**7**) was found higher compared to unsubstituted zinc(II) phthalocyanine in DMSO (Figure 10, inset). The singlet oxygen generation properties of other metallo-phthalocyanines (**4**, **5,** and **6**) studied in

this work did not investigate due to paramagnetic behavior of the used Co, Ni, and Cu metal ions the cavities of these phthalocyanines because paramagnetic metal ions reduce the photoactivity of the molecules.

The synthesis of the phthalocyanine compounds bearing different alkylthio groups on the phthalocyanine ring were given in the literature but the photochemical properties of these derivatives were studied limitedly. On the other hand, the phthalocyanine derivatives substituted at the nonperipheral octa positions of the phthalocyanine macrocycle are very rare in the literature. The studied zinc(II) phthalocyanine (7) showed higher singlet oxygen production in comparison with other octa nonperipheral substituted photosensitizers containing different alkylthio groups such as 2-propoxy, benzyloxy or 3,5 bis(benzyloxy)benzyloxy groups [39]. Similarly, the studied zinc(II) phthalocyanine (7) showed higher singlet oxygen production in comparison with alkylthio substituted pyridoporphyrazines [40]. Additionally, the phthalocyanine 7 exhibited similar singlet oxygen generation when compared to the nonperipherally octa-sulfanyl substituted zinc phthalocyanine [41].

3.6. Photodegradation studies

Photodegradation quantum yield can be used to study the stability of photosensitizer during the photocatalytic reaction in PDT [42]. The current study shows that photodegradation properties of studied zinc(II) phthalocyanine (**7**) were determined in DMSO by monitoring the collapse of their absorption bands underused light irradiation with increasing time (Figure 11). The Φ_d value of zinc(II) phthalocyanine was found the order of 3.79×10^{-5} (between 10^{-3} and 10^{-6} for ideal photosensitizer) in DMSO [21]. The Φ_d value of the investigated zinc(II) phthalocyanine (**7**) was found slightly higher than unsubstituted zinc(II) phthalocyanine ($\Phi_d = 2.61 \times 10^{-5}$) [18]. On the other hand, the phthalocyanine 7 exhibited lower photodegredation quantum yield value when compared to the non-peripherally octa-sulfanyl substituted zinc phthalocyanine [41] which means that the studied zinc(II) phthalocyanine (7) exhibited higher stability to light irradiation.

4. Conclusion

In this study, the phthalonitrile derivative substituted with 3-hydroxypropylthio groups at 3 and 6 positions as ligand and its non-peripheral octa substituted metallo-phthalociyanines [M =Zn(II), Ni(II), Cu(II) and Co(II)] were synthesized and characterized. Electrochemical properties of the proposed compounds also investigated because of these kinds of compounds show the possible potential usage in electro-catalysis, electrosensing, and electrochromic devices. When the ΔE values in Table 3 are compared, the **ZnPc** compound is electrically more conductive than phthalonitrile. In this electrical conductivity, zinc(II) plays an important role. Besides, the molecular geometry and GIAO ^{1}H and ^{13}C NMR chemical shift values of the molecule in the ground state had been estimated by applying B3LYP with 6–31G(d,p) basis set. Also, the photochemical properties such as singlet oxygen generation and photodegradation under light irradiations were studied for the determination of possible photosensitizer ability of zinc(II) phthalocyanine derivative **7**. These properties of the other studied metallo-phthalocyanines did not investigate because of the paramagnetic behavior of metal ions (Co, Ni, and Cu) in the cavities of these phthalocyanines. The absorbance of the new zinc(II) phthalocyanine (**7**) was studied in DMSO solutions at different concentrations for determination of the most suitable concentration for further photochemical properties. The singlet oxygen production of this phthalocyanine (**7**) was determined in DMSO using a chemical method. The singlet oxygen production of studied zinc(II) phthalocyanine (**7**) was found higher compared to unsubstituted zinc(II) phthalocyanine in DMSO. In this study, the photodegradation behavior of the zinc(II) phthalocyanine (**7**) was determined in DMSO. The Φ_d value of zinc(II) phthalocyanine was found in the order of 3.79×10^{-5} in DMSO. This value is slightly higher than unsubstituted zinc(II) phthalocyanine [37,43].

Acknowledgments

The authors are grateful to Pamukkale University–PAUBAP (Project No. 2020HZDP002) as they supported this project financially.

References

1. Torre GD, Vazquez P, Agullo-Lopez F, Torres T. Phtahlocyanines and related compounds: Organic targets for nonlinear optical applications. Journal of Materials Chemistry 1998; 8: 1671-1683. doi: 10.1039/A803533D

2. Leznoff CC, Lever ABP. Phthalocyanines Properties and Applications 3. New York, NY, USA: Wiley-VCH, 1993.

3. Leznoff CC, Lever ABP. Phthalocyanines Properties and Applications 1. New York, NY, USA: Wiley-VCH, 1989.

4. Parra V, Bouvet M, Brunet J, Rodríguez-Méndez ML, Saja JA. On the effect of ammonia and wet atmospheres on the conducting properties of different lutetium bisphthalocyanine thin films. Thin Solid Films 2008; 5: 9012-9019. doi: 10.1016/j.tsf.2007.11.092

5. Bouvet M. Phthalocyanine-based field-effect transistors as gas sensors. Analytical and Bioanalytical Chemistry 2006; 384: 366-373. doi: 10.1007/s00216-005-3257-6

6. Yang F, Forrest SR. Photocurrent generation in nanostructured organic solar cells. ACS Nano 2008; 2 (5): 1022-1032. doi: 10.1021/nn700447t

7. Forrest SR. Ultrathin organic films grown by organic molecular beam deposition and related techniques. Chemical Review 1997; 97 (6): 1793-1896. doi: 10.1021/cr941014o

8. Leznoff CC, Lever ABP. Phthalocyanines Properties and Applications 2. New York, NY, USA: Wiley-VCH, 1993.

9. Bilgin A, Ertem B, Gök Y. Synthesis and characterization of new metal-free and metallophthalocyanines containing spherical or cylindrical macrotricyclic moieties. Polyhedron 2005; 24: 1117-1124. doi: 10.1016/j.poly.2005.01.025

10. Leznoff CC, Lever ABP. Phthalocyanines Properties and Applications 4. New York, NY, USA: Wiley-VCH, 1996.

11. Emmelius M, Pawlowski G, Vollmann HW. Materials for optical data storage, Angewandte Chemie International Edition 1989; 28 (11): 1445-1471. doi: 10.1002/anie.198914453.

12. Yılmaz F, Özer M, Kani İ, Bekaroğlu Ö. Catalytic activity of a thermoregulated, phase-seperable Pd(II)-perfluoroalkylphthalocyanine complex in an organic/fluorous biphasic system: hydrogenation of olefins. Catalysis Letters 2009; 130: 642-647. doi: 10.1007/s10562-009-9959-1

13. Rosenthal I. Phthalocyanines as photodynamic sensitizers. Photochemistry and Photobiology 1991; 53 (6): 859-870.doi: 10.1111/j.1751-1097.1991.tb09900.x

14. Özçeşmeci İ, Okur Aİ, Gül A. New phthalocyanines bearing tetra(hydroxylethylthio) functionalities. Dyes and Pigments 2007; 75(3): 761-765. doi: 10.1016/j.dyepig.2006.08.003

15. Necedova MM, Martinicka A, Magdolen P, Novakova V, Zahradnik P. Phthalocyanine-triphenylamine dyads: synthesis, electrochemical, spectral and DFT study. Dyes and Pigments 2017; 141: 448-456.doi: 10.1016/j.dyepig.2017.02.025

16. Wannebroucq A, Meunier-Prest R, Chambron JC, Braxhais CH, Suisse JM et al. Synthesis and characterization of fluorophthalocyanines bearing four 2-(2-thienyl)ethoxy moieties: from the optimization of the fluorine substitution to chemosensing. RCS Advances 2017; 7: 41272-41281. doi: 10.1039/c7ra05325hrsc.li/rsc-advances

17. Tuncer S, Koca A, Gül A, Avcıata U. 1,4-Dithiaheterocycle-fused porphyrazines: Synthesis, characterization, voltammetric and spectroelectrochemical properties. Dyes and Pigments 2009; 81 (2): 144-151. doi: 10.1016/j.dyepig.2008.09.022

18. Gurol I, Durmuş M, Ahsen V, Nyokong T. Synthesis, photophysical and photochemical properties of substituted zinc phthalocyanines. Dalton Transactions 2007; 34: 3782-3791.doi: 10.1039/B704345G

19. TaratulaO, Schumann C, Nalewey MA, Pong AJ, Chan KJ, et al.A multifunctional theronostic platform based on phthalocyanine-loaded dendrimer for imge-guided drug delivery and phthadynamictheraphy. Molecular Pharmaceuties 2013; 10 (10): 3946-3958. doi: 10.1021/mp400397t

20. Shao J, Dai Y, Zhao W, Xie J, Xue J et al. Intracellular distribution and mechanism of photosensitizer Zn(II)-phthalocyanine solubilized in cremophor EL against human hepatocellular carcinoma HepG2 cells. Cancer Letters 2013; 330 (1): 49-56. doi: 10.1016/j.canlet.2012.11.017

21. Durmuş M. Photochemical and photophysical charactrization. In: Nyokong T, Ahsen V (editors). Photosensitizers in Medicine, Environment and Security. New York, NY, USA: Springer, 2012, pp. 135-266.

22. Wang R, Zhao Y, Zhu C, Huang X. New Synthesis of 3,6-dibromophthalonitrile and phthalocyanine having eight thienyl substituents at peripheral α-positions. Journal of Heterocyclic Chemistry 2015; 52 (4): 1230-1233. doi: 10.1002/jhet.2130

23. Baygu Y, Gök Y. A highly water-soluble zinc(II) phthalocyanines as potential for PDT studies: synthesis and characterization. Inorganic Chemistry Communication 2018; 96: 133-138. doi: 10.1016/j.inoche.2018.08.004

24. Nyokong T. Structure and Bonding: Functional Phthalocyanine Molecular Materials. Berlin, Germany: Springer, 2010, pp. 45-88.

25. Kobayashi N, Furuyama T, Satoh K. Rationally designed phthalocyanines having their main absorption band beyond 1000 nm. Journal of the American Chemical Society 2011; 133 (49): 19642-19645. doi: 10.1021/ja208481q

26. Huhey JE. Inorganic Chemistry. New York, NY, USA: Harper Int. Ed., 1978, pp. 16.

27. Furuyama T, Satoh K, Kushiya T, Kobayashi N. Design, synthesis, and properties of phthalocyanine complexes with main-group elements showing main absorption and fluorescence beyond 1000 nm. Journal of the American Chemical Society 2014; 136 (2): 765-776. doi: 10.1021/ja411016f

28. Koçan H, Burat AK. Synthesis and characterization of [7-(trifluoromethyl)-quinolin-4-yl] oxy-substituted phthalocyanines. Monatshefte für Chemie 2013; 144: 171-177. doi: 10.1007/s00706-012-0790-9

29. Engelkamp H, Nolte RJM. Molecular materials based on crown ether functionalized phthalocyanines. Journal of Porphyrins and Phthalocyanine 2000; 4 (5): 454-459. doi: 10.1002/1099-1409(200008)4:5<454::AID-JPP261>3.0.CO;2-D

30. Nas A, Biyiklioglu Z, Fandaklı S, Sarkı G, Yalazan H et al. Tetra(3-(1,5-diphenyl-4,5-dihydro-1H-pyrazol-3-yl)phenoxy) substituted cobalt, iron and manganese phthalocyanines: synthesis and electrochemical analysis. Inorganica Chimica Acta 2017; 466: 86-92. doi: 10.1016/j.ica.2017.05.050

31. Hanabusa K, Shirai H. Catalytic functions and application of metallophthalocyanine polymers. ChemInform 1993; 24 (43): 197-222. doi: 10.1002/chin.199343294

32. Elgrishi N, Rountree KJ, McCarthy BD, Rountree ES, Eisenhart TT et al. A practical beginner's guide to cyclic voltammetry. Journal of Chemical Education 2018; 95 (2): 197-206. doi: 10.1021/acs.jchemed.7b00361

33. Francl MM, Pietro WJ, Hehre WJ. Self-consistent molecular orbital methods, XXIII. A polarization-type basis set for second-row elements. The Journal of Chemical Physics 1982; 77 (7): 3654-3665. doi: 10.1063/1.444267

34. Hariharan PC, Pople JA. The influence of polarization functions on molecular orbital hydrogenation energies. Theoretica Chimica Acta 1973; 28: 213-222. doi: 10.1007/BF00533485

35. Figgen D, Rauhut G, Dolg M, Stoll H. Energy-consistent pseudopotentials for group 11 and 12 atoms: adjustment to multi-configuration Dirac–Hartree–Fock data. Chemical Physics 2005; 311 (1-2): 227-244. doi: 10.1016/j.chemphys.2004.10.005

36. Peterson KA, Puzzarini C. Systematically convergent basis sets for transition metals. II. pseudopotential-based correlation consistent basis sets for the group 11 (Cu, Ag, Au) and 12 (Zn, Cd, Hg) elements. Theoretical Chemistry Accounts 2005; 114: 283-296. doi: 10.1007/s00214-005-0681-9

37. Yıldız B, Baygu Y, Kara I, Dal H, Gök Y. The synthesis, characterization and computational investigation of new metalloporphyrazine containing 15-membered S_4 donor macrocyclic moieties. Tetrahedron 2016; 72 (44): 6972-6981. doi:10.1016/j.tet.2016.09.028

38. Shao W, Wang H, He S, Shi L, Peng K et al. Photophysical properties and singlet oxygen generation of three sets of halogenated corroles. Journal of Physical Chemistry B 2012; 116 (49): 14228-14234. doi: 10.1021/jp306826p

39. Tillo A, Stolarska M, Kryjewski M, Popenda L, Sobotta L et al. Phthalocyanines with bulky substituents at non-peripheral positions-synthesis and physico-chemical properties. Dyes and Pigments 2016; 127: 110-115. doi: 10.1016/j.dyepig.2015.12.017

40. Sakamoto K, Watabiki S, Yoshino S, Komoriya T. Synthesis of alkylthio substituted pyridoporphyrazines and their photophysicochemical properties. Journal of Porphyrins and Phthalocyanines 2017; 21: 658-664. doi: 10.1142/S1088424617500626

41. Tekdaş DA, Kumru U, Gürek AG, Durmuş M, Ahsen V et al. Towards near-infrared photosensitisation: a photosensitising hydrophilic non-peripherally octasulfanyl-substituted Zn phthalocyanine. Tetrahedron Letters 2012; 53: 5227-5230. doi: 10.1016/j.tetlet.2012.07.062

42. Erdoğmuş A, Durmuş M, Uğur AL, Avciata O, Avciata U et al. Synthesis, photophysics, photochemistry and fluorescence quenching studies on highly soluble substituted oxo-titanium(IV) phthalocyanine complexes. Synthetic Materials 2010; 160 (17-18): 1868-1876. doi: 10.1016/j.synthmet.2010.07.002

43. Baygu Y, Yıldız B, Kara I, Dal H, Gök Y. Synthesis, characterization and computational investigation of novel metalloporphyrazines containing 15-memberedO_2S_2-donor macrocyclic moieties. Journal of Porphyrins and Phtalocyanines 2018; 22: 207-220. doi: 10.1142/S1088424618500104

Supplementary materials

1. Materials and methods

1.1. Experimental

All reagents were supplied from commercial suppliers. All reactions were carried out under the argon atmosphere. All solvents were dried and purified according to standard methods [S1]. ^{1}H NMR and ^{13}C NMR spectra were measured by a Varian Mercury 300 NMR spectrometer. FT-IR and mass spectra were recorded on a Perkin-Elmer Spectrum One FT-IR spectrometer and on a micrOTOF mass spectrometer. UV-Vis spectral measurements were performed by Shimadzu UV-1601 spectrometer at room temperature. Melting points were measured by an electrothermal apparatus and are uncorrected. 3,6-dibromo phthalonitrile was synthesized according to the literature procedures [S2].

2. Synthesis

2.1. 3,6-bis-(3-hydroxypropylthio)phthalonitrile (3)

A mixture of 3,6-dibromo phthalonitrile (**1**) (1.43 g, 5 mmol), excess amount of anhydrous Na_2CO_3 (2.65 g, 25 mmol) and 3-mercapto-1-propanol (**2**) (1.15 g, 12.5 mmol) in dry DMF (25 mL) were placed in a round-bottom two flask under argon atmosphere. This suspension was stirred at 50 °C for 10 h. The reaction mixture was monitored by TLC [silica gel (chloroform:methanol)(95:5)]. At the end of this period, the reaction mixture was cooled to room temperature and filtered. The filtrate was evaporated under reduced pressure to dryness and then the solid product purified by column chromatography on silica gel using the mixture of chloroform:methanol (95:5) as eluent to give a pale yellow solid. Yield: 0.58 g (38%); m.p. 143 °C (140 °C in reference [S3]). FT-IR (ν, cm^{-1}): 3236 (O-H), 3067 (Ar-H), 2929–2848 CH_2), 2220 (C≡N), 1527, 1471, 1434, 1284, 1143, 1035, 822; ^{1}H NMR (300 MHz, DMSO-d_6): δ 7.81–7.78 (d, 2H, Ar-H), 3.49 (m, 4H, OCH_2), 4.67 (s, 2H, OH), 3.17 (m, 4H, S-CH_2), 1.73 (m, 4H, CH_2). ^{13}C NMR (75 MHz, DMSO-d_6): δ 145.3, 141.2, 132.9, 116.9, 59.6, 31.9, 29.7. Anal. calcd. for $C_{14}H_{16}N_2S_2O_2$: C, 54.52; H, 5.23; N, 9.08. Found: C, 54.33; H, 5.40; N, 9.23.

2.2. 1,4,8,11,15,18,22,25-octakis(3-hydroxypropylthio)phthalocyaninato metal complexes (4–7)

A mixture of 0.5 mmol (0.154 g) 3,6-bis-(3-hydroxypropylthio)phthalonitrile and 0.182 mmol anhydrous metal salt (23.7 mg cobalt chloride, 23.7 mg nickel chloride, 24.5 mg copper (II) chloride or 33.3 mg zinc acetate) in 3 mL of *n*-pentanol and 3 drops 1,8-diazabicyclo[5.4.0]undec-7-ene (DBU) was heated and stirred at 155 ˚C for 24 h under an argon atmosphere in a Schlenk tube. After this time, the mixture was chilled out to room temperature and the precipitate was filtered off and then washed subsequently with chloroform, water, and acetone. After that, the products were purified by Soxhlet extraction with chloroform and then dried in vacuo over dried $MgSO_4$.

2.2.1. Cobalt (II) phthalocyanine(4)

Yield: 0.105 g (65%); m.p. > 300 ˚C. FT-IR (**ν**, cm^{-1}): 3238 (-OH), 3057 (Ar-H), 2923–2868 (alkyl-CH), 1690 (C=N), 1567, 1434, 1281, 1153, 1041, 928; UV-Vis $\boldsymbol{\lambda}_{max}$ (nm) (log **ε**) in DMSO: 767 (4.54), 701 (4.24), 377 (4.33), 283 (4.59). MS: *m/z* 1291.03 $[M]^+$ (calculated MS: 1291.2) . Anal. calcd. for $C_{56}H_{64}N_8O_8S_8Co$; C, 52.03; H, 4.99; N, 8.67. Found: C, 51.86; H, 4.69; N, 8.40%.

2.2.2. Copper (II) phthalocyanine(5)

Yield: 0.102 g (63%); m.p. > 300 ˚C. FT-IR **ν** (cm^{-1}): 3290 (-OH), 3057 (Ar-H), 2923–2868 (alkyl-CH), 1644, 1585, 1427, 1280, 1154, 1036; UV-Vis $\boldsymbol{\lambda}_{max}$ (nm) (log **ε**) in DMSO: 797 (4.79), 713 (4.27), 503 (3.88), 349 (4.49), 283 (4.88). MS: *m/z* 1297.2 $[M+2]^+$, 1358.1 $[M+K+Na+H]^+$ (calculated MS: 1295.2) . Anal. calcd. for $C_{56}H_{64}N_8O_8S_8Cu$; C, 51.85; H, 4.97; N, 8.64; found: C, 51.34; H, 4.72; N, 8.36%.

2.2.3. Nickel (II) phthalocyanine(6)

Yield: 0.115 g (71%); m.p. > 300 ˚C. FT-IR **ν** (cm^{-1}): 3241 (-OH), 3048 (Ar-H), 2929– 2875 (alkyl-CH), 1690, 1567, 1434, 1281, 1153, 1041; ^{1}H NMR (300 MHz, DMSO-d_6): 7.74–7.58 (br s, 8H, ArH), 4.70 (br s, 8H, OH), 3.66 (m, 16H, OCH_2), 3.33 (m, 16H, SCH_2, with d-DMSO proton), 1.95 (m, 16H, CH_2CH_2). ^{13}C NMR (75 MHz, DMSO-d_6): 145.5, 133.1, 131.7, 124.7, 60.4, 32.0, 28.1. UV-Vis $\boldsymbol{\lambda}_{max}$ (nm) (log **ε**) in DMSO: 811 (4.56), 736 (4.14), 525 (3.62), 363 (4.27), 300 (4.85). MS: *m/z* 1291.9 $[M+2]^+$, 1309.6 $[M+H_2O]^+$ (calculated MS: 1290.2). Anal. calcd. for $C_{56}H_{64}N_8O_8S_8Ni$; C,52.04; H, 4.99; N, 8.67; found: C, 51.65; H, 4.74; N, 8.38%.

2.2.4. Zinc (II) phthalocyanine(7)

Yield: 0.125 g (77%); m.p. > 300 ˚C. FT-IR **ν** (cm^{-1}): 3254 (-OH), 3052 (Ar-H), 2924– 2868 (alkyl-CH), 1644, 1557, 1435, 1280, 1142, 1041, 919; ^{1}H NMR (300 MHz, DMSO-d_6): 7.98 (s, 8H, ArH), 4.75 (s, 8H, OH), 3.77–3.76 (d, 16H, OCH_2),

3.45 (br s, 16H, SCH_2), 2.11 (m, 16H, CH_2CH_2). ^{13}C NMR (75 MHz, DMSO-d_6): 152.7, 133.7, 132.7, 125.57, 60.4, 32.3, 28.2. UV-Vis λ_{max} (nm) (log ε) in DMSO: 792 (4.88), 711 (4.34), 503 (3.75), 346 (4.46), 296 (4.85). MS: *m/z* 1298.9 $[M+3]^+$ (calculated MS: 1296.2). Anal. calcd. for $C_{56}H_{64}N_8O_8S_8Zn$; C, 51.78; H, 4.97; N, 8.63; found: C, 52.24; H, 4.77; N, 8.52%.

2.3. Electrochemical measurements

All electrochemical measurements were actualized with Ivium potentiostat using the three-electrode system at room temperature. The Pt and Ag wires were used as counter and reference electrodes, respectively. Optically transparent indium tin oxide (ITO) coated glass slides from Delta Technologies (7 × 50 × 0.5 mm thickness and 8 – 12 ohm.sq^{-1}) were used as a working electrode. Electrochemical characterizations of the materials were carried out in DCM/DMF (0.8 / 0.2) solution containing 0.1 M tetrabutylammonium hexafluorophosphate (TBP_6). The cyclic voltammetry technique was applied for the electrochemical characterization of materials. The ITO-coated glass electrode, Ag wire, and Pt wire have been plunged into the electrochemical cell. Different voltage has been applied on the working electrode through the potentiodynamic method and has been controlled using the Ivium Compact stat. The Ag wire electrode was calibrated versus Ag/AgCl (3M KCl) electrode.

2.4. Photochemical studies

2.4.1. Singlet oxygen quantum yields

Singlet oxygen production determinations were carried out using the experimental set-up described in the literature [S4]. Typically, a 3 mL portion of the respectively substituted zinc(II) phthalocyanine (**7**) solution (concentration = 1 × 10^{-5} M) containing the singlet oxygen quencher was irradiated in the Q band region with the photo-irradiation set-up described in the reference [S4]. Singlet oxygen production was determined in the air using the relative method using unsubstituted ZnPc as a standard. 1,3-diphenylisobenzofuran (DPBF) was used as a chemical quencher for singlet oxygen in DMSO. To avoid chain reactions induced by DPBFin the presence of singlet oxygen [S5],the concentration of quenchers (DPBF) was lowered to ~ 3 × 10^{-5} M. Solutions of sensitizer (1 × 10^{-5} M) containing DPBF was prepared in the dark and irradiated in the Q-band region using the setup described and degradation of DPBF at 417 nm was monitored.

2.4.2. Photodegradation quantum yields

Photodegradation quantum yield (Φ_d) determinations were carried out using the experimental set-up described in the literature [S4]. Photodegradation quantum yields were determined using Equation (1),

$$\Phi_d = \frac{(C_0 - C_t).\ V\ .\ N_A}{I_{abs}\ .\ S\ .\ t} \quad (1)$$

where C_0 and C_t are the sample (**7**) concentration before and after irradiation respectively, V is the reaction volume, N_A is the Avogadro's constant, S is the irradiated cell area, it is the irradiation time and I_{abs} is the overlap integral of the radiation source light intensity and the absorption of the sample (**7**). A light intensity of 2.17 × 10^{16} photons s^{-1} cm^{-2} was employed for Φ_d determinations.

2.5. Theoretical calculations

Density functional theory (DFT) is one of the most useful quantum chemistry tools in calculating the ground state properties of compounds. In the modeling, the initial guess of the compound was provided from the X-ray coordinates. The molecular structures were optimized to get the global minima by using DFT/B3LYP/6-31G (d,p) level in the gas phase. The electronic properties were also calculated using 6-31G(d,p) and 6-31G+(d, p) levels. All the calculations were carried out with the Gaussian 16 B.01 [S6] package program and GaussView 6.0.16 [S7] was used for the visualization of the structure. The ^1H and ^{13}C NMR chemical shielding constants were calculated using GIAO-B3LYP in the gas phase and DMSO. For the NBO analysis, the same calculation procedure in the gas phase was also used. The ^1H and ^{13}C-NMR chemical shifts were converted to the TMS scale by subtracting the calculated absolute chemical shielding of TMS ($d = \Sigma_0 - \Sigma$), where d is the chemical shift, Σ is the absolute shielding and Σ_0 is the absolute shielding of TMS, whose values (reference shielding for ^1H and ^{13}C) are at 31.883 ppm and 191.80 ppm, respectively, for B3LYP/6-31G(d,p). Besides, molecular electrostatic potential (MEP) of the title molecules were investigated by B3LYP/6-31G(d,p). The energy difference between HOMO and LUMO levels was described as the optical bandgap for the HOMO to LUMO excitation energy (TDDFT) and the electronic band gap for excitation energy difference (ΔE = LUMO-HOMO). The visible absorption maxima of the molecule were corresponded to the electron transition from HOMO to LUMO by using calculations of molecular orbital geometry.

3. ^{1}H NMR, ^{13}C NMR, FT-IR, MS spectra and optimize geometric parameters of the ZnPc

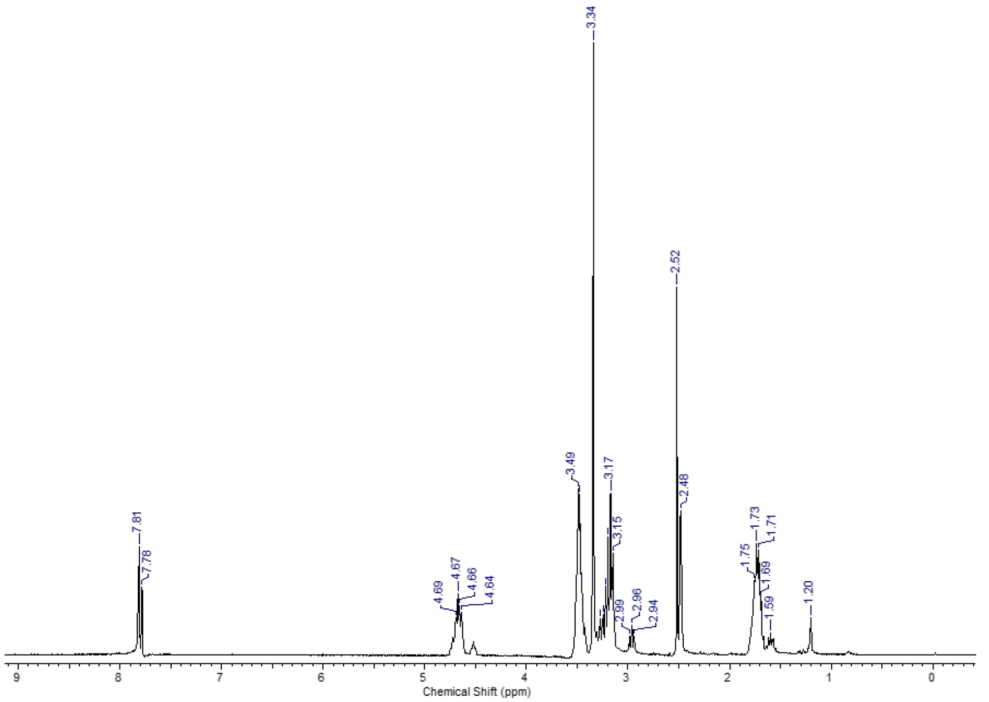

Figure S1. ^{1}H-NMR spectrum of 3,6-bis-(3-hydroxypropylthio)phthalonitrile (**3**) in DMSO-d_6.

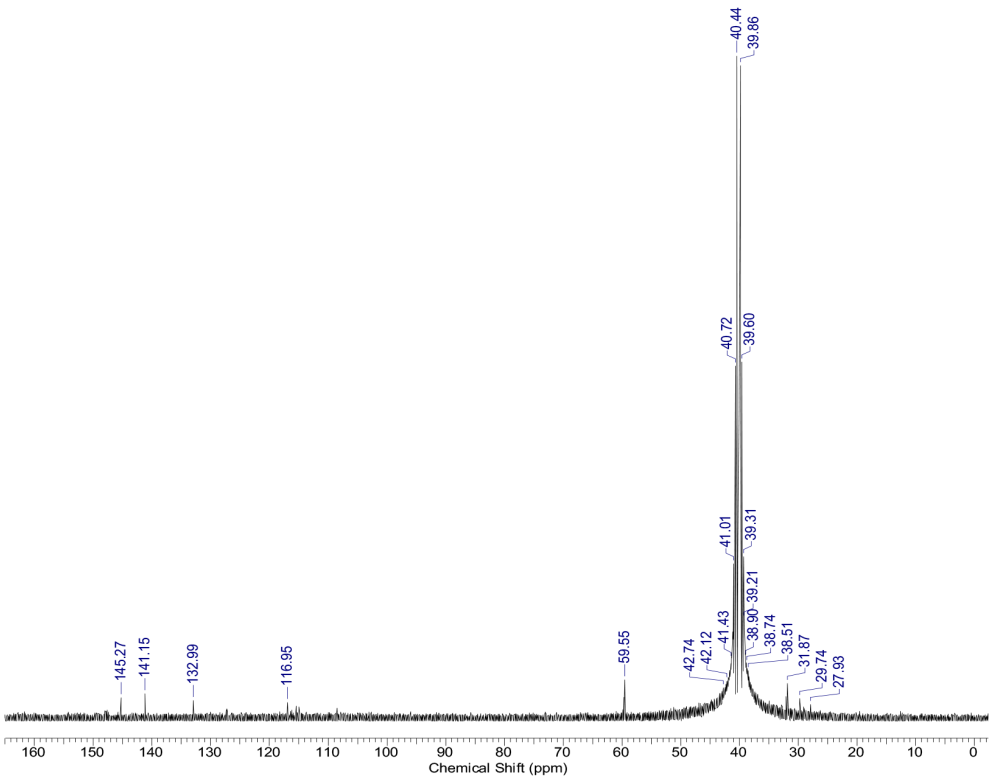

Figure S2. ^{13}C-NMR spectrum of 3,6-bis-(3-hydroxypropylthio)phthalonitrile (**3**) in DMSO-d_6.

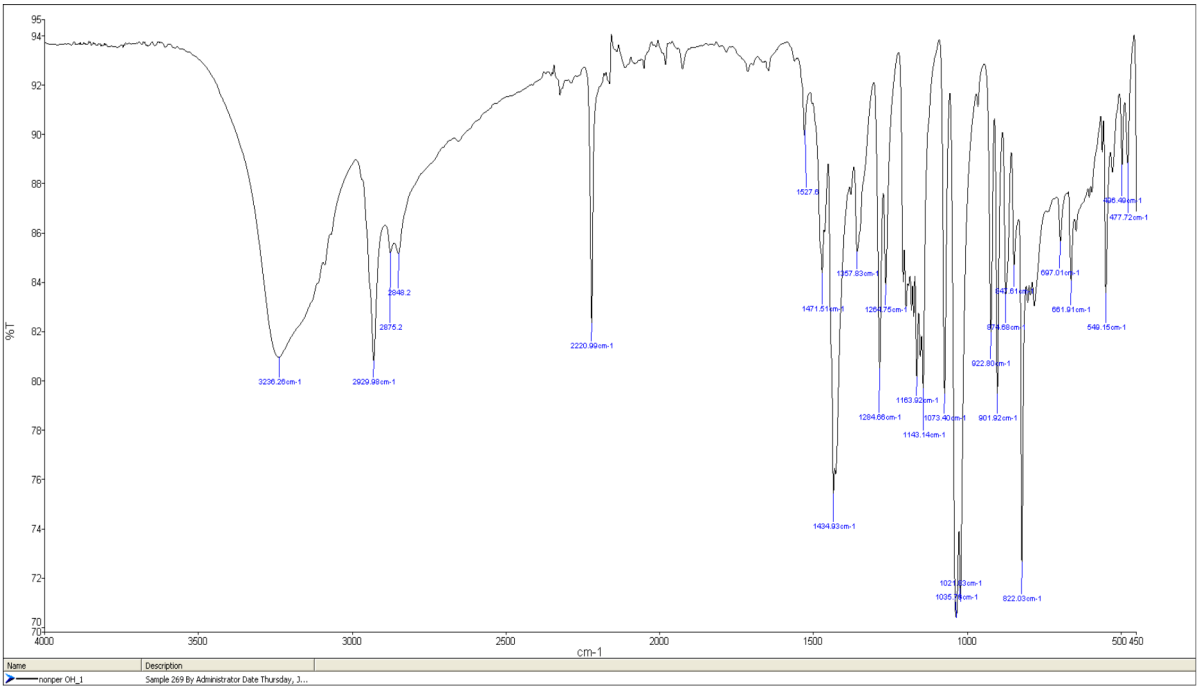

Figure S3. FT-IR spectrum of 3,6-bis-(3-hydroxypropylthio)phthalonitrile (**3**).

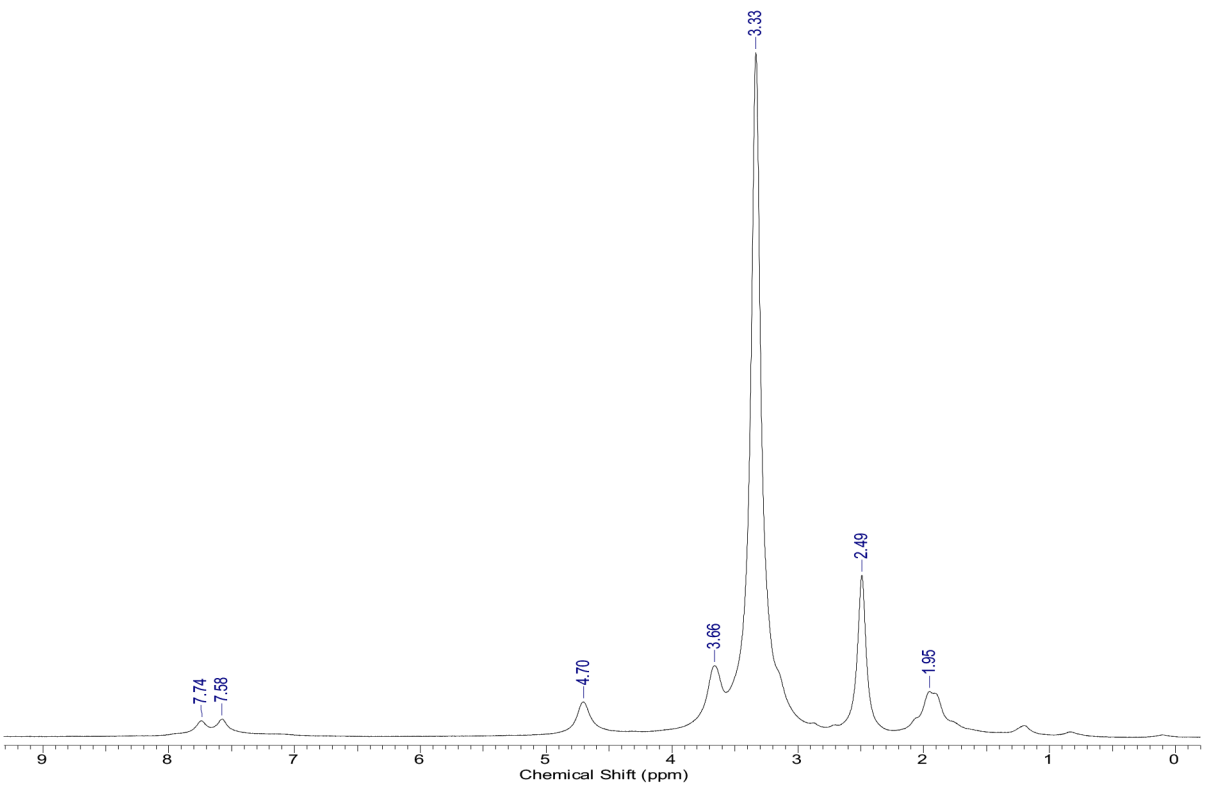

Figure S4. ^{1}H-NMR spectrum of **NiPc** in DMSO-d_6.

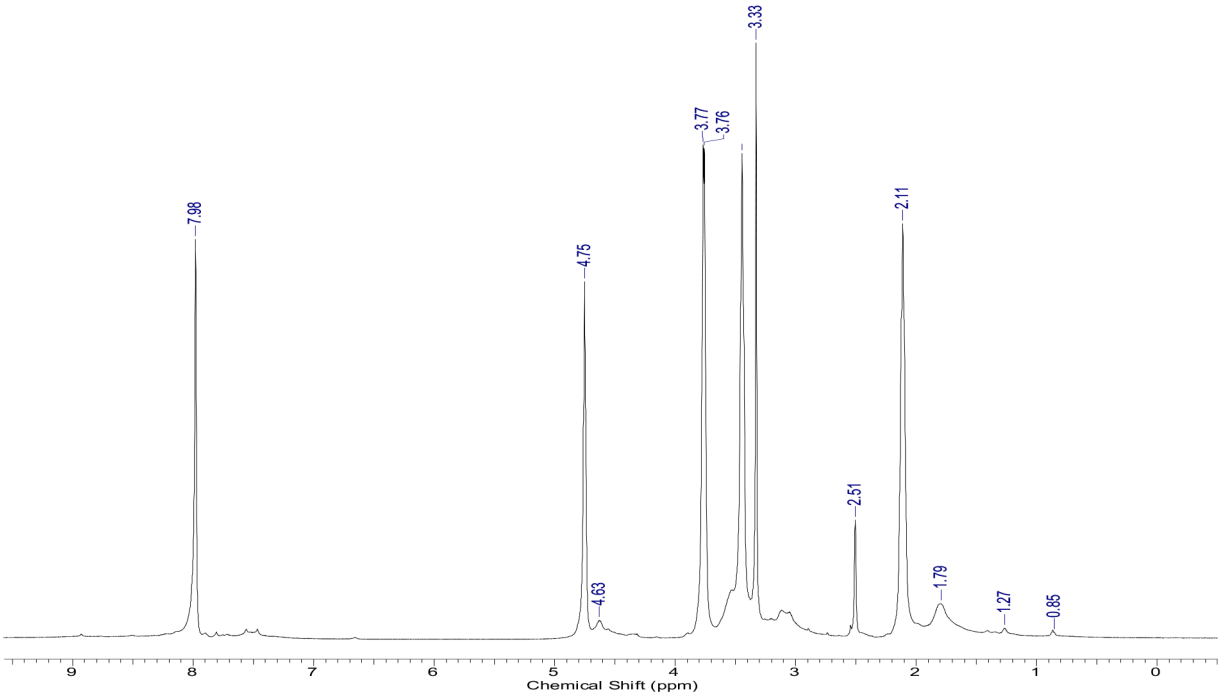

Figure S5. ^{1}H-NMR spectrum of **ZnPc** in DMSO-d_6.

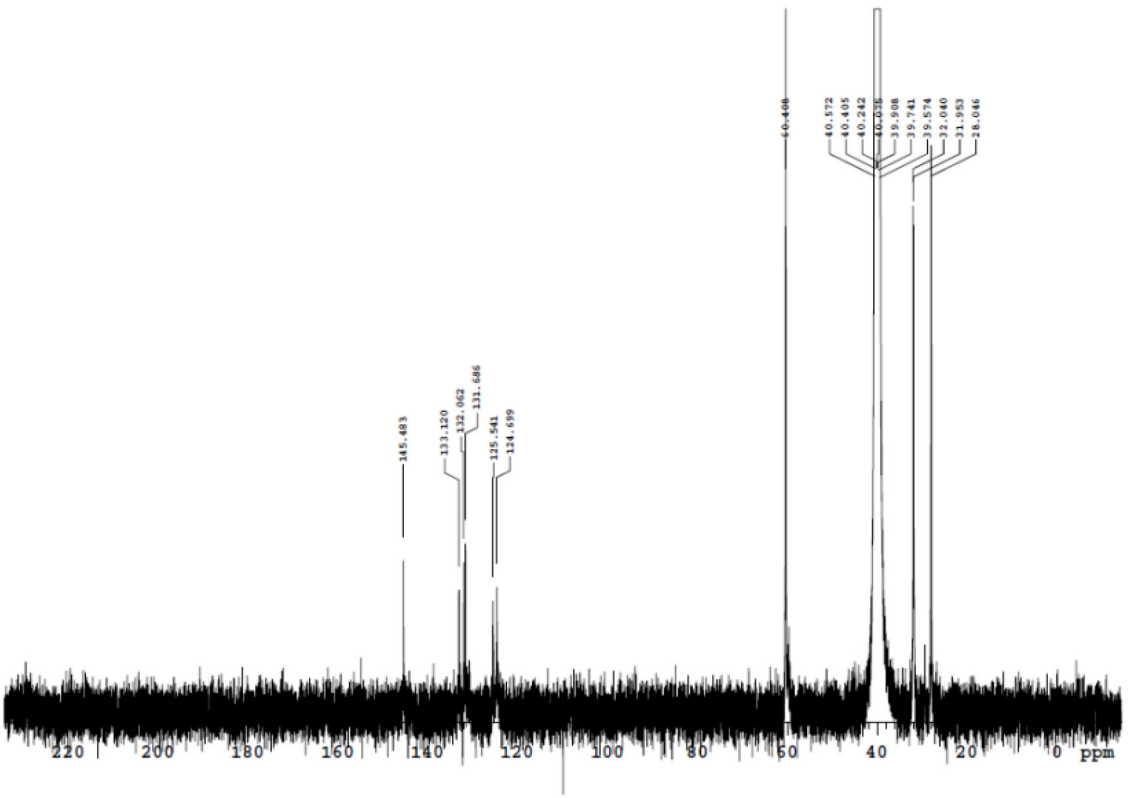

Figure S6. ^{13}C-NMR spectrum of **NiPc** in DMSO-d_6.

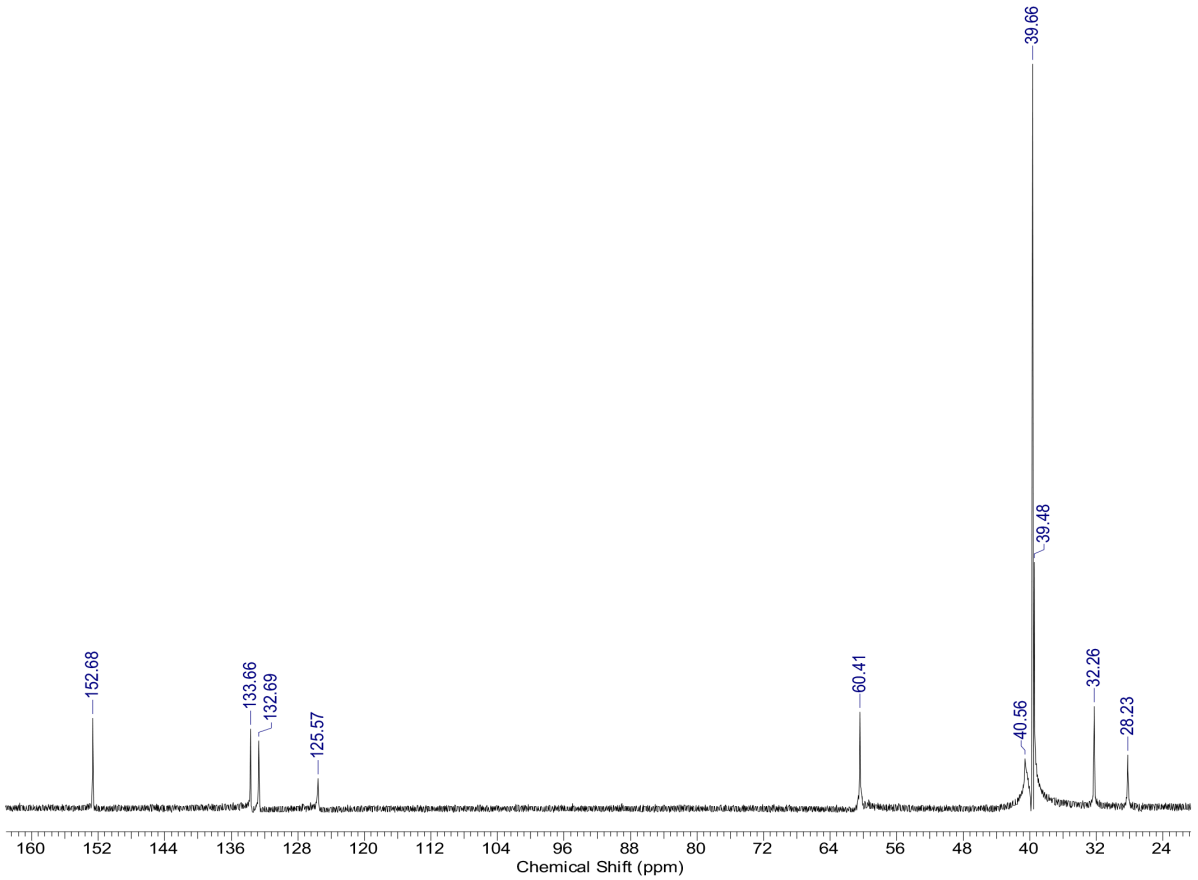

Figure S7. ^{13}C-NMR spectrum of **ZnPc** in DMSO-d_6.

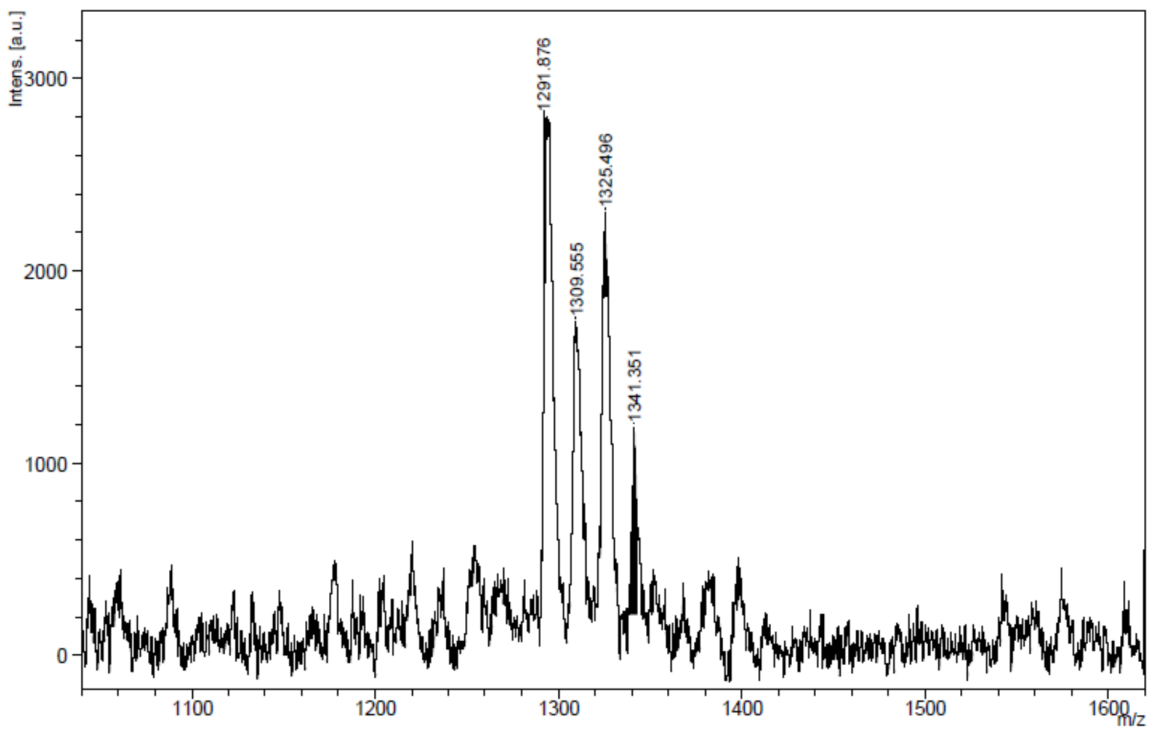

Figure S8. Mass spectrum of **NiPc** (MALDI-TOF).

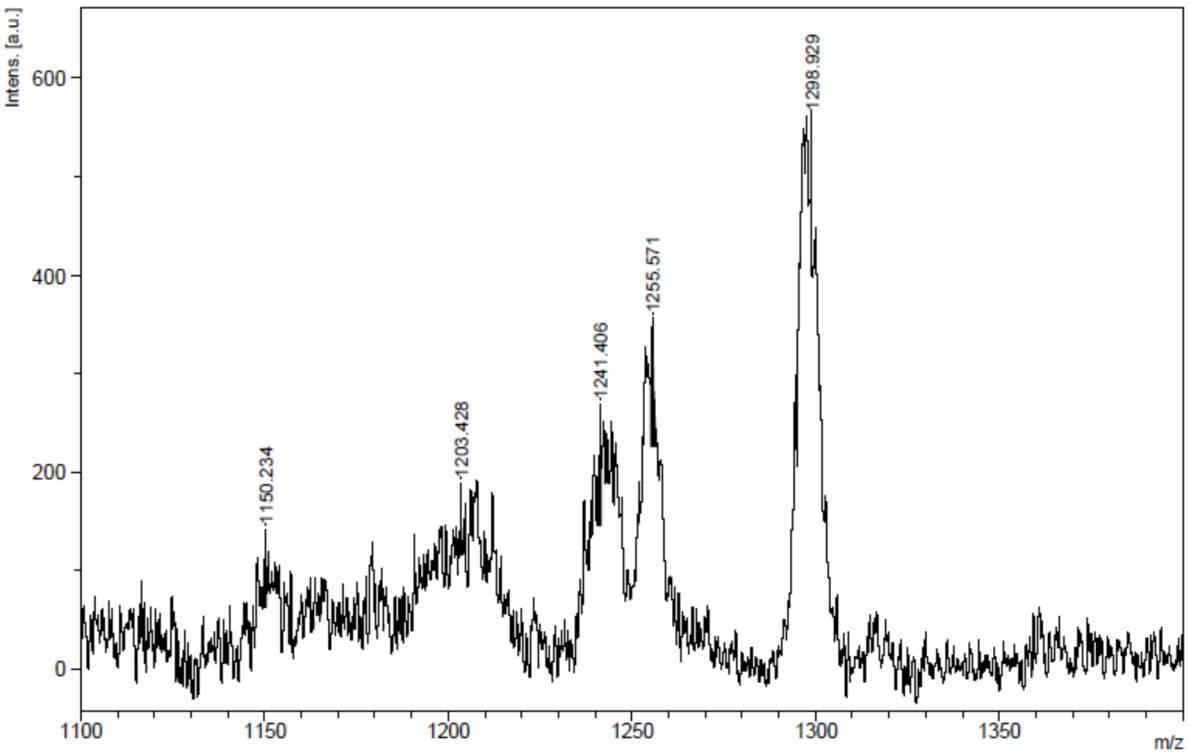

Figure S9. Mass spectrum of **ZnPc** (MALDI-TOF).

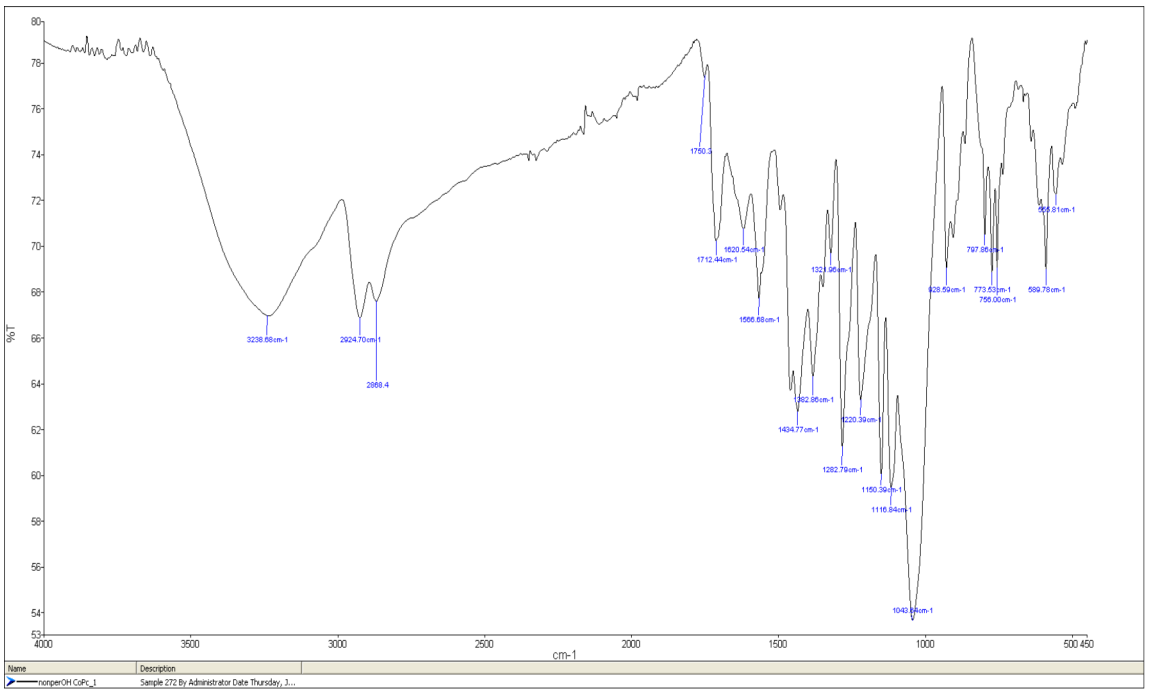

Figure S10. FT-IR spectrum of **CoPc**.

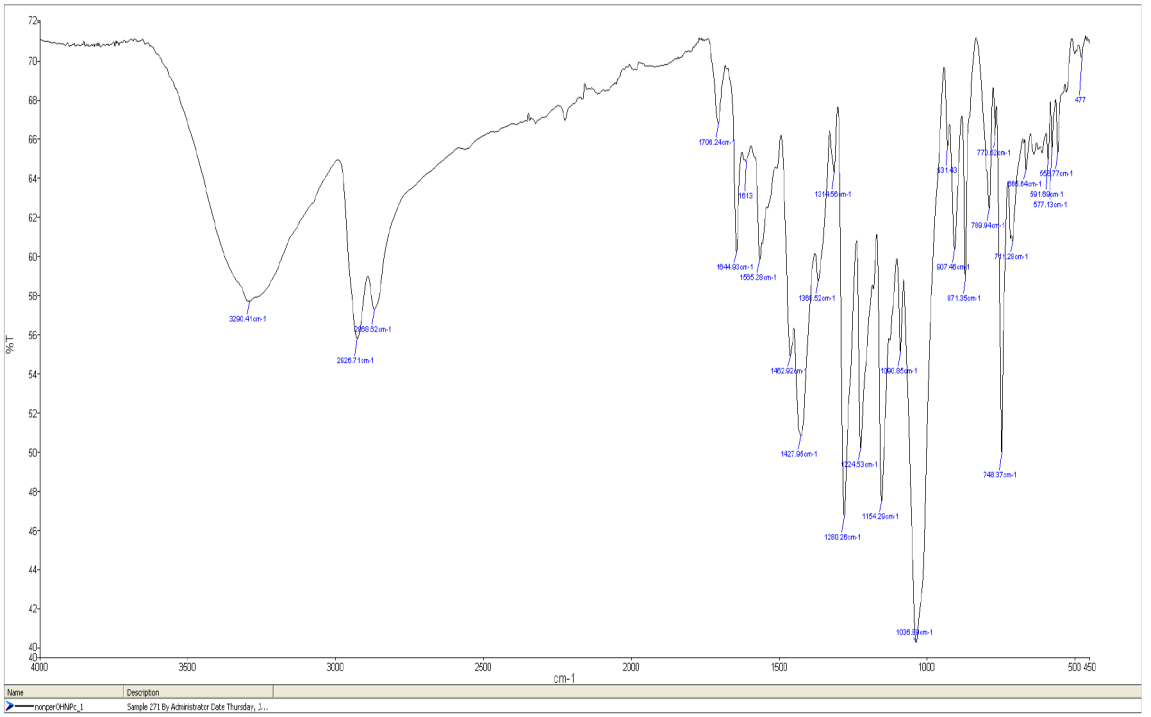

Figure S11. FT-IR spectrum of **CuPc**.

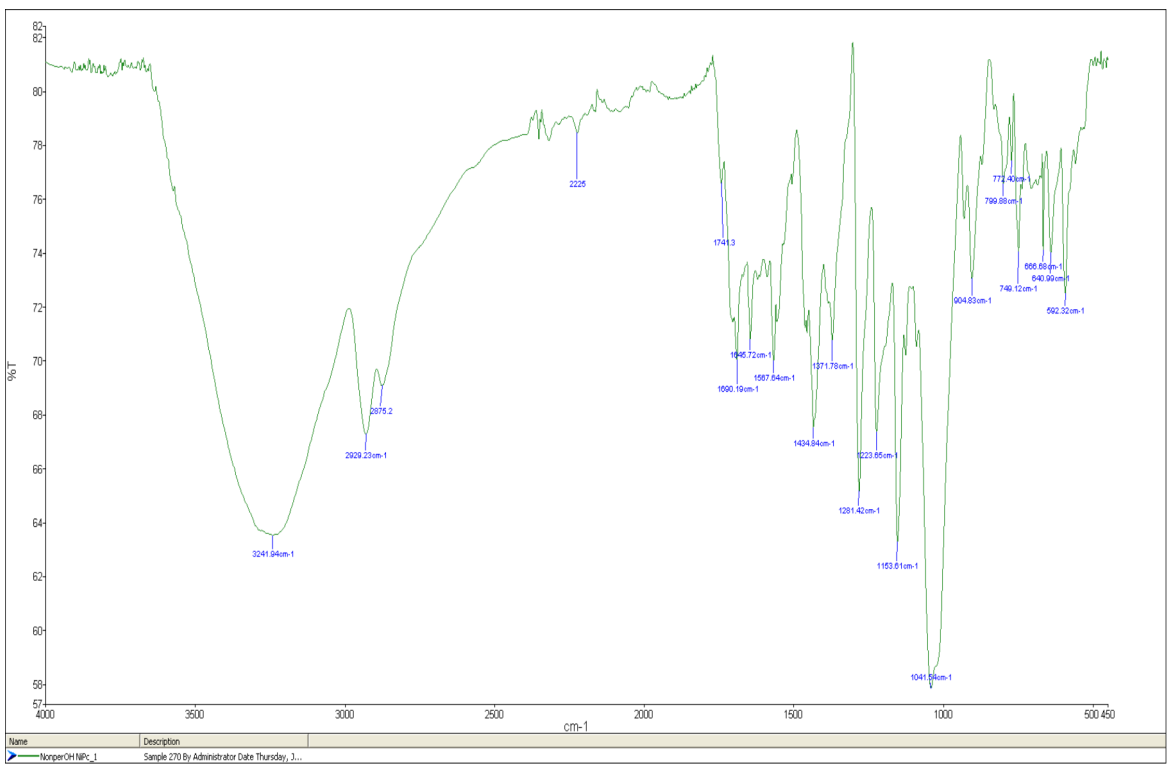

Figure S12. FT-IR spectrum of **NiPc**.

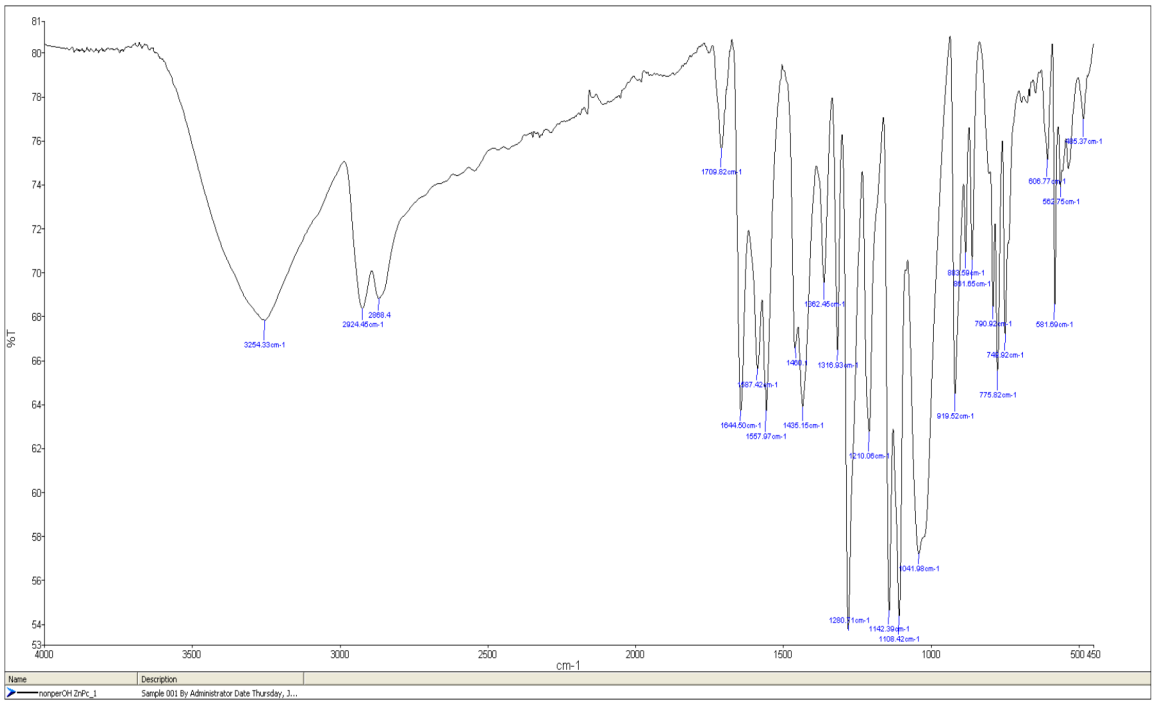

Figure S13. FT-IR spectrum of **ZnPc**.

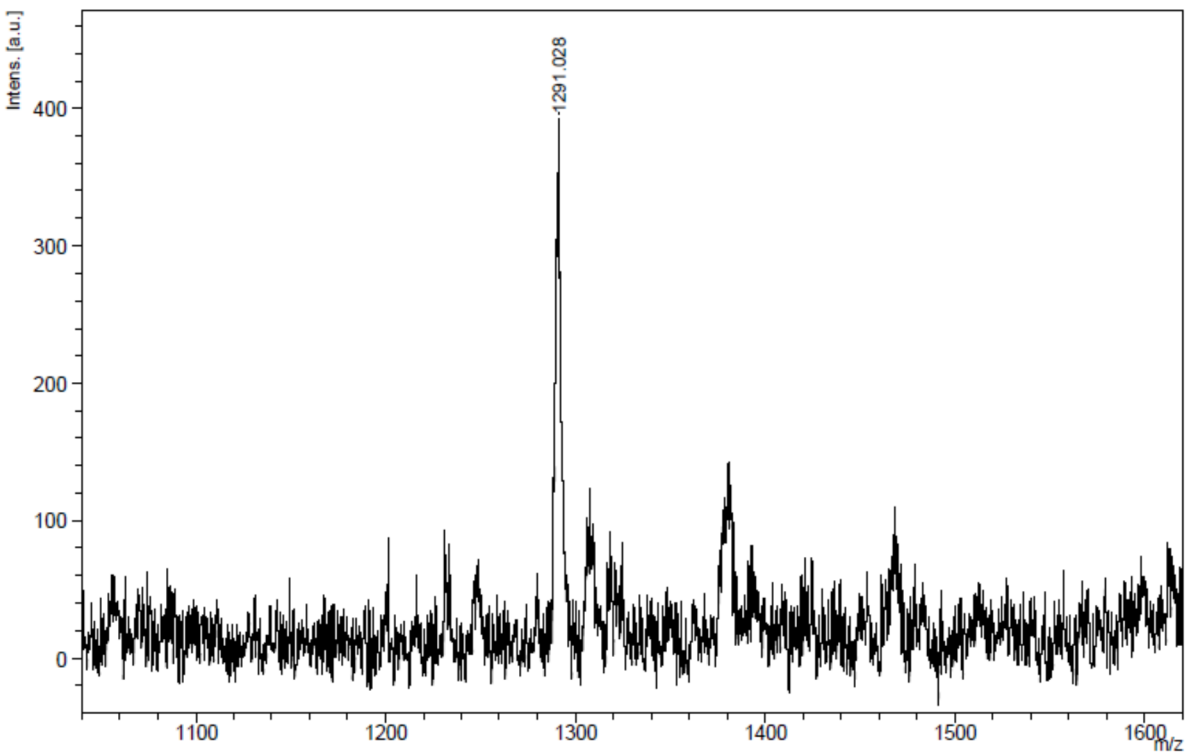

Figure S14. Mass spectrum of **CoPc** (MALDI-TOF).

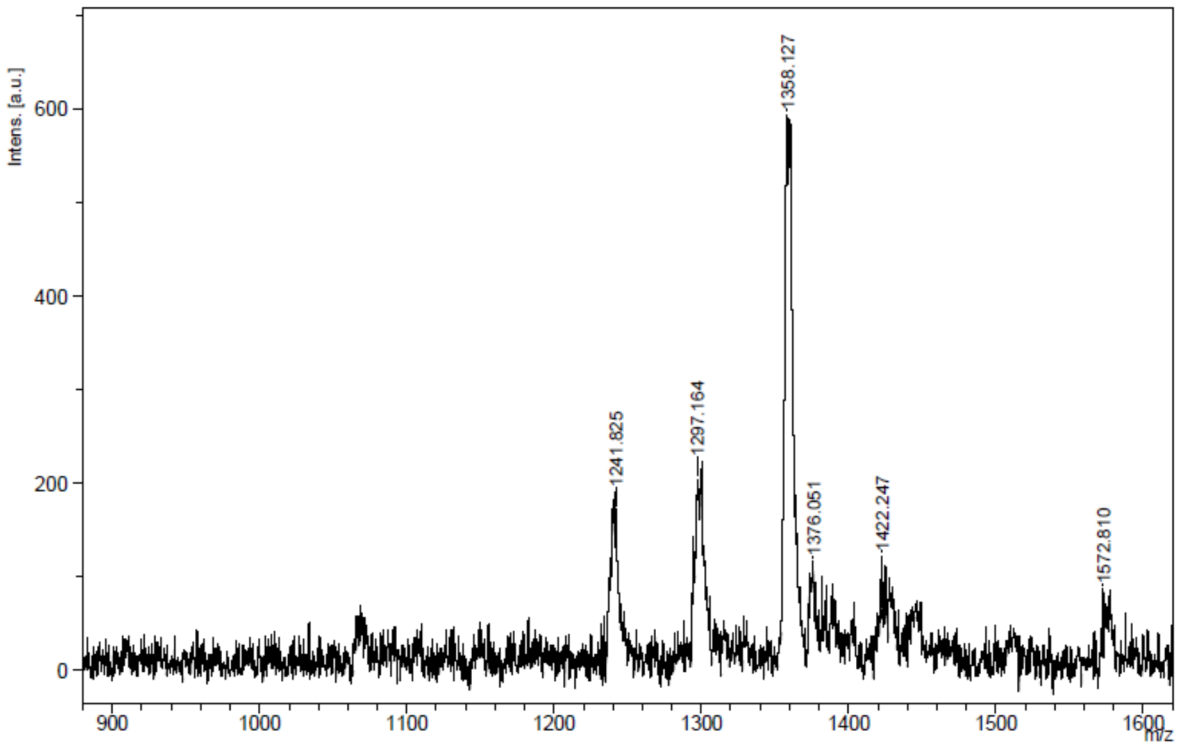

Figure S15. Mass spectrum of **CuPc** (MALDI-TOF).

Table S1. Selected optimized geometric parameters of the **ZnPc** in the ground state.

Bond lengths	(Å)	Bond Angles	(°)	Dihedral angles	(°)
C3-N5	1.33	C3-N7-Zn145	124.35	C14-N16-Zn145-N10	–173.72
N5-C20	1.33	C4-N7-Zn145	124.38	C19-N22-Zn145-N7	–173.71
C4-N6	1.33	C8-N10-Zn145	124.39	C8-N10-Zn145-N16	–171.47
C13-N15	1.33	C9-N10-Zn145	124.36	C4-N7-Zn145-N22	–171.45
C8-N21	1.33	C13-N16-Zn145	124.16	C2-C9-N10-Zn145	–162.30
N6-C14	1.33	C14-N16-Zn145	124.33	C2N3-N3-N7-Zn145	–162.25
C9-N15	1.33	C19-N22-Zn145	124.33	C11-C13-N16-Zn145	–160.86
C19-N21	1.33	C20-N22-Zn145	124.16	C18-C20-N22-Zn145	–160.84
C3-N7	1.37	N7-Zn145-N16	89.96	N21-C19-N22-Zn145	–22.14
C8-N10	1.37	N7-Zn145-N22	90.03	N6-C14-N16-Zn145	–22.14
C4-N7	1.37	N10-Zn145-N16	90.04	N6-C4-N7-Zn145	–20.43
C19-N22	1.37	N10-Zn145-N22	89.96	N21-C8-N10-Zn145	–20.40
C20-N22	1.37			C20-N22-Zn145-N7	–11.15
C13-N16	1.37			C13-N16-Zn145-N10	–11.14
C14-N16	1.37			N3-N7-Zn145-N22	–7.85
C9-N10	1.37			C9-N10-Zn145-N16	–7.82
N22-Zn145	1.99			C8-N10-Zn145-N22	8.44
N7-Zn145	1.99			C4-N7-Zn145-N16	8.46
N10-Zn145	1.99			C14-N16-Zn145-N7	10.41
N16-Zn145	1.99			C19-N22-Zn145-N10	10.42
				N15-C9-N10-Zn145	20.17
				N5-N3-N7-Zn145	20.22
				N15-C13-N16-Zn145	22.62
				N5-C20-N22-Zn145	22.65
				C17-C19-N22-Zn145	160.99
				C12-C14-N16-Zn145	161.01
				C24-C4-N7-Zn145	162.19
				C1-C8-N10-Zn145	162.23
				N3-N7- n145-N16	172.07
				C9-N10-Zn145-N22	172.10
				C20-N22-Zn145-N10	172.99
				C13-N16-Zn145-N7	172.99

Table S2. ^{1}H and ^{13}C chemical shift values of the **ZnPc** compound.

Atoms	Exp	Gas-phase	DMSO
C73, C74, C75, C72, C76, C77, C78, C79,	28.23	33.48	34.1
C57, C58, C61, C62, C63, C64, C59, C60	32.26	32.36	32.78
C97, C98, C99, C102, C103, C104	60,41	63.14	62.96
C1, C2, C11, C12, C17, C18, C23, C24	125.57	130.46	130.59
C25, C28, C29, C30, C31, C32, C33, C34	132.69	135.07	134.94
C26, C27, C35, C36, C37, C38, C39, C40	133.66	117.07	119.32
C3, C4, C13, C14, C8, C9, C19, C20	152.68	148.46	149.21
H81, H114, H82, H113, H83, H120, H96, H119, H95, H118, H94, H117, H84, H116, H80, H115	2.11	2.46	2.19
H122, H124, H126, H128, H130, H132, H134, H136	4.75	0.19	0.75
H66, H85, H86, H87, H65, H88, H89, H71, H70, H90, H69, H91, H68, H92, H67, H93	3.45	3.07	3.19
H107, H139, H106, H140, H109, H141, H105, H142, H110, H143, H111, H144, H108, H137, H112, H138	3.77	4.07	4.08
H41, H42, H43, H44, H45, H46, H47, H48	7.98	7.79	7.99

Table S3. Second order perturbation theory analysis of Fock matrix in NBO for the **ZnPc** in gas phase at B3LYP/6-31G(d,p).

Bond	Occupancy	Hybrid (p % ch.)	Acceptor (j)	Occupancy	Hybrid (p %ch.)	$E(^2)^a$ (kcal/mol)	$E(j)-E(i)^b$ (a.u.)	$F(i.j)^c$ (a.u.)
C1-C2(π)	1.62025	p	π *(C9-N15)	0.45979	p	4.26	1.21	0.064
			σ *(C28-S49)	0.03155	$Sp^{2.66}$	4.05	0.87	0.053
			σ * (C8-N10)	0.04379	$Sp^{2.24}$	28.39	0.22	0.075
C8-N10 (σ *)	0.04379	$Sp^{2.24}$	π* (C1-C 2)	0.46887	p	68.90	0.05	0.073
			π* (C9-N15)	0.45979	p	91.22	0.03	0.060
			π*(C19-N21)	0.45985	p	190.70	0.03	0.087
C9-N15(π)	1.70502	p	π*(C13-N16)	0.58427	p	35.59	0.28	0.097
C20-N22(π)	1.76914	p	π*(C20-N22)	0.58427	p	32.10	0.32	0.096
C3-N5 (π*)	0.45979	p	π*(C23-C31)	0.46530	p	219.59	0.02	0.078
C 4-N7 (π*)	0.58474	p	π*(C3-N5)	0.45979	p	91.22	0.03	0.060
			π*(N6-C14)	0.45985	p	190.70	0.03	0.087
			π*(C24-C32)	0.46530	p	99.63	0.04	0.080
C9-N15(π*)	0.45979	p	π*(C1-C2)	0.46887	p	118.85	0.02	0.070
C13-N16 (π*)	0.58427	p	π*(N6-C 14)	0.45985	p	91.52	0.03	0.060
			π*(C9-N15)	0.45979	p	191.05	0.03	0.087
			π*(C11-C34)	0.46132	p	97.65	0.04	0.080
C19-N21 (π*)	0.45985	p	π*(C17-C29)	0.46132	p	209.25	0.02	0.078
C20-N22(π*)	0.58427	p	π*(C3-N5)	0.45979	p	191.04	0.03	0.087
			π*(C18-C30)	0.46132	p	97.65	0.04	0.080
			π*(C19-N21)	0.45985	p	91.52	0.03	0.060
C25-C26 (π*)	0.40404	p	π*(C1-C2)	0.46887	p	275.24	0.01	0.079
C27-C28 (π*)	0.40404	p	π*(C1-C2)	0.46887	p	275.24	0.01	0.079
N6 (LP1)	1.86832	$Sp^{3.13}$	σ*(C4-N7)	0.04379	$Sp^{2.24}$	14.48	0.80	0.098
			σ*(C14-N16)	0.04373	$Sp^{2.25}$	14.55	0.80	0.099
S 49 (LP2)	1.82989	p	π*(C 27-C28)	0.40404	p	20.52	0.25	0.068
S 56 (LP2)	1.83354	p	π* (C12-C33)	0.46132	p	18.28	0.25	0.066

$E^{(2)\,a}$ means energy of hyperconjugative interaction; ^{b}energy difference between donor and acceptor i and j NBO orbital; $F(i,j)^c$ is the Fock matrix element between i and j NBO orbitals.

References

S1. Perrin DD, Armarego WLF. Purification of Laboratory Chemicals. 2nd ed. Oxford, UK: Pergamon Press, 1980.

S2. Wang R, Zhao Y, Zhu C, Huang X. New synthesis of 3,6-dibromophthalonitrile and phthalocyanine having eight thienyl substituents at peripheral α-positions. Journal of Heterocyclic Chemistry 2015; 52 (4): 1230-1233. doi: 10.1002/jhet.2130

S3. Baygu Y, Gök Y. A highly water-soluble zinc(II) phthalocyanines as potential for PDT studies: synthesis and characterization. Inorganic Chemistry Communication 2018; 96: 133-138. doi: 10.1016/j.inoche.2018.08.004

S4. Durmuş M. Photochemical and Photophysical Charactrization. In: Nyokong T, Ahsen V (editors). Photosensitizers in Medicine, Environment and Security. New York, NY, USA: Springer, 2012, pp. 135-266.

S5. Spiller W, Kliesch H, Wöhrle D, Hackbarth S, Schnurpfeil G. Singlet oxygen quantum yields of different photosensitizers in polar solvents and micellar solutions. Journal of Porphyrins and Phthalocyanines 1998; 2 (2): 145-158. doi: 10.1002/(SICI)1099-1409(199803/04)2:2<145::AID-JPP60>3.0.CO;2-2

S6. Frisch MJ, Trucks GW, Schlegel HB, Scuseria GE, Robb MA et al. Gaussian 16, revision B.01. Wallingford, CT, USA: Gaussian Inc., 2016.

S7. Dennington RD, Keith TA, Millam JM. GaussView 6.0.16. Shawnee, KS, USA: Semichem, Inc., 2000-2016.